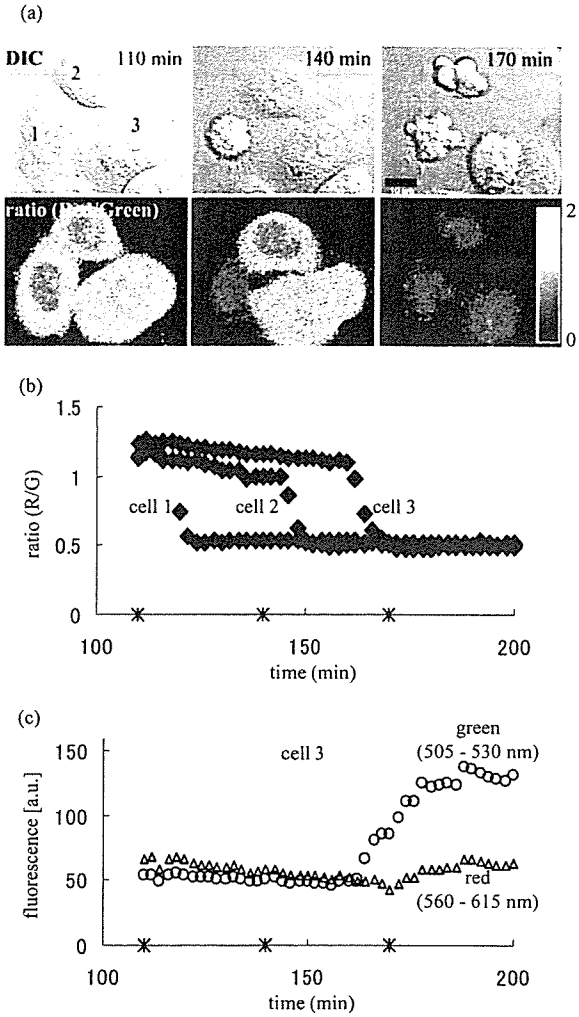

Fig. 3. Real-time imaging of caspase activation in living HeLa cells during cell death. HeLa cells expressing GR-sensor were treated with TNF-α/CHX, and fluorescent images were obtained every 2 min. a: DIC images (upper panels) and fluorescent ratios (Red/Green, lower panels) are shown in grayscale. The indicated time represents the time after the addition of TNF-α/CHX. Scale bar, 10 μm. b: The fluorescent ratio of cells were plotted. Cell 1, 2, or 3 corresponds to the cells shown in panel a. c: The mean pixel intensity in arbitrary fluorescent units (a.u.) for each channel was plotted. The fluorescence of cell No. 3 from panel a is shown. Open circle, GFP; open triangle, DsRed; closed diamond, ratio of Red/Green. Asterisks on the x-axis indicate the time points of the images in panel a.

point of the reduction of the fluorescent ratio as follows: the start point was the point after which the value decreased over four continuous points or more, the value decreased more than 10% in total, and the reduction of the value was not because of artificial noise such as focus shift; the end point followed the start point and was the point at which the value stopped decreasing. The sensitivity of the probe was calculated as $\Delta R = |(R_{end} - R_{start}) / R_{start}|$, where R_{start} and R_{end} were the fluorescent ratio at the start point and the end point, respectively. Figure 4 shows ΔR for each probe. GR and YR, as well as CY, showed the highest ΔR. They each showed a more than 50% change during cell death. CR showed a slightly lower ΔR, but its change was still 44% on average. CG and GY were less sensitive, probably because the fluorescent spectra of the donor and the acceptor were so similar that our system could not effectively measure FRET between them. CY *vs* GR, CY *vs* YR, or GR *vs* YR were not significantly different, and any other comparisons were significantly different by the Games-Howell test ($P<0.05$).

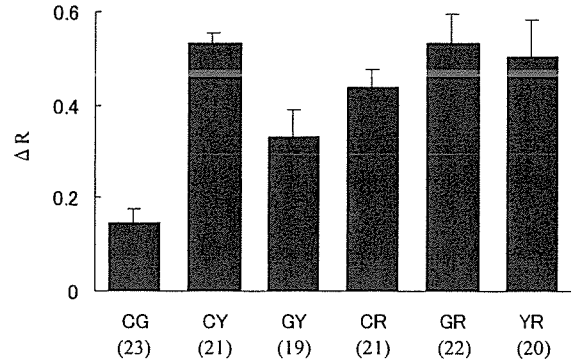

Fig. 4. Comparison of the sensitivity of various caspase-sensors. The amount of change of the fluorescent ratio during cell death (ΔR) was determined in each cell as described in the text. Bars represent means ± S.D. The number of cells used in each analysis is shown in parentheses.

Simultaneous multi-event analysis using two FRET probes

Finally, we tried to perform multi-FRET measurement. We constructed a YR-initiator caspase sensor and a CR-effector caspase sensor by changing the caspase substrate sequence in the sensor and applied them to real-time imaging analysis simultaneously in order to reveal the temporal relationships between the initiator caspase activation and the effector caspase activation in the same cell. The caspase substrate sequences were derived from procaspase-3 and PARP, respectively, and their sequences are shown in Fig. 5a. These sensors were cleaved mainly by caspase-8/9 and caspase-3, respectively (11).

Simultaneous measurement of these sensors was performed under the multi-track scanning mode, in which two sets of excitation-detection conditions were used alternatively. CFP fluorescence by excitation at 458 nm was measured in the first track, and YFP and DsRed fluorescence by excitation at 488 nm was mea-

(a) YFP-SGLDCGIETDSGVDEPVAT-DsRed : YR-(IC)sensor
CFP-SGKRKGDEVDGVDEPVAT-DsRed : CR-(EC)sensor

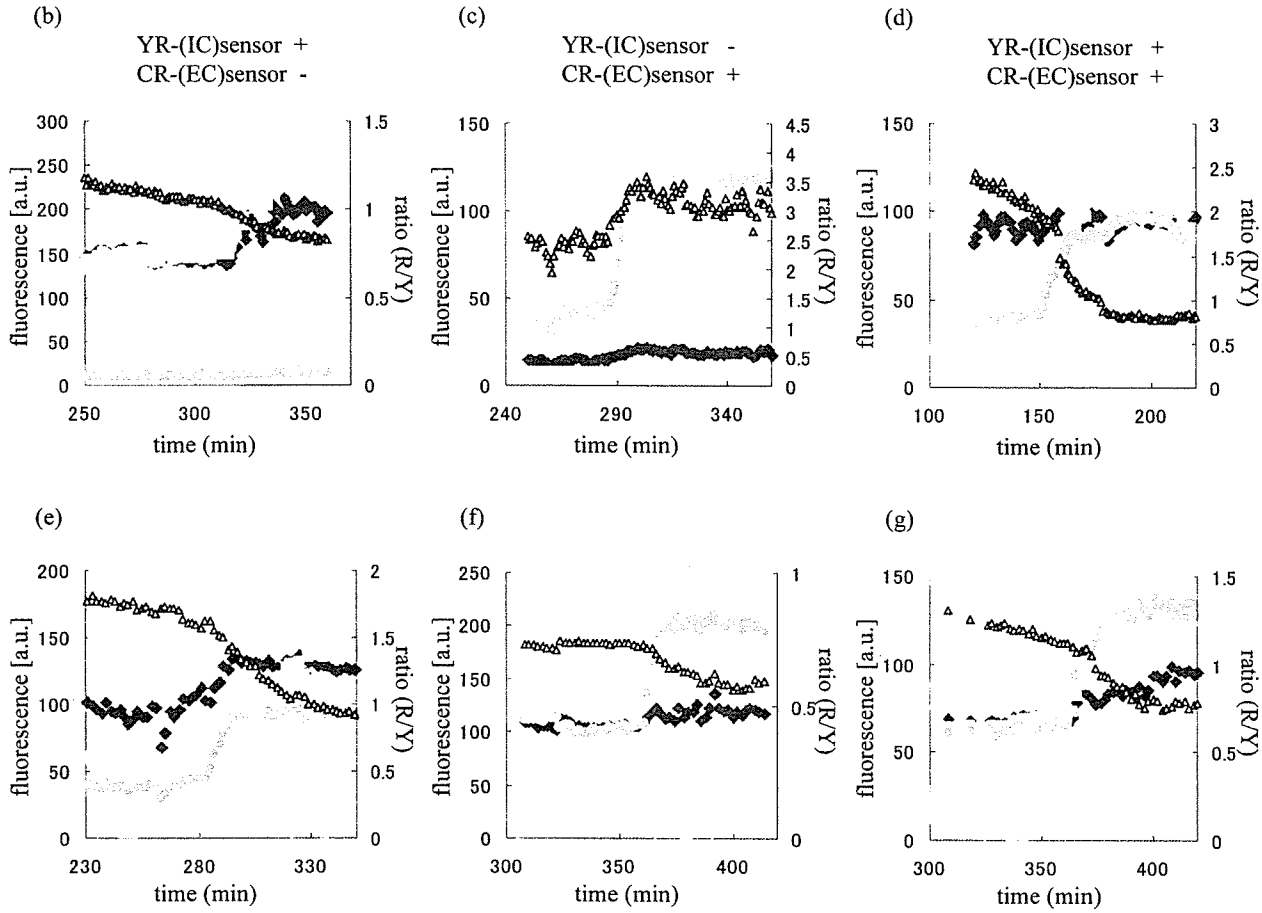

Fig. 5. Simultaneous measurement of initiator- and effector-caspase activation with YR-sensor and CR-sensor. HeLa cells expressing YR-initiator caspase sensor and/or CR-effector caspase sensor were treated with TNF-α/CHX and observed as described in the text. a: Probes used in this study. Underline indicates peptide derived from procaspase-3 and PARP, and bold indicates the consensus 4 amino acid sequence for caspase recognition. b – g: Cells expressing YR-initiator caspase sensor (b), CR-effector caspase sensor (c), or both of them (d – g) were treated with TNF-α/CHX. The fluorescence of CFP, YFP, and DsRed (colored plots) and the fluorescent ratio of DsRed/YFP (open triangles) were plotted against time after TNF-α/CHX treatment.

sured in the second track. The time difference of scanning between tracks is about 3 – 8 s. Figures 5b and 5c show control studies with cells expressing only one of the probes. These control studies were conducted in the same conditions as Fig. 5d. Figures 5b and 5c indicate that the YR- and CR-sensor could detect initiator- and effector-caspase activation as an increase of YFP and CFP signal, respectively, and the contamination of the signal between the YFP and CFP channels was negligible. So, we used an increase of the YFP and CFP signal as index of the initiator- and the effector-caspase activation, respectively. The DsRed signal in Fig. 5c was derived from direct excitation of DsRed in the CR-sensor by the excitation light at 488 nm and was increased when the cell shrank because fluorescent proteins were concentrated in the cell.

Figure 5d shows typical data of multi-probe analysis with the YR-initiator caspase sensor and CR-effector caspase sensor. In this cell, the fluorescence was dramatically changed at 150 – 160 min after TNF-α /CHX treatment. The YFP and CFP signal began to increase almost simultaneously, suggesting that initiator caspase and effector caspase were initially activated within a short time period. Figures 5e – 5g show three

other examples. We observed more than 30 cells in at least 3 independent experiments and found that all dying cells showed similar results.

Discussion

In this study, we developed various color versions of caspase-sensors with CFP, GFP, YFP, and DsRed and revealed that various combinations are applicable in FRET analysis. CY, CR, GR, and YR pairs are preferable FRET pairs that possess a high ability to detect the caspase activation.

The sensitivity shown in Fig. 4 represents the apparent FRET change that depends on the measuring system and was determined by three factors. 1) Intrinsic FRET efficiency: All 4 fluorescent proteins had different fluorescent characteristics; therefore, the levels of FRET efficiency in 6 probes differed from each other. 2) Excitation crosstalk: The acceptors were excited directly by the excitation light. 3) Emission crosstalk: The acceptor channel was contaminated with the donor signal, and vice versa, because the setting shown in Table 1 could not perfectly separate the signals from the donor and the acceptor. The differences in these factors cause the difference of sensitivity among the sensors. Factors 2) and 3) reduce the apparent FRET change in the measurement. In the case of the CG-sensor, for example, fluorescent spectrum of donor and acceptor are so similar that the intrinsic FRET efficiency may be high, but excitation and emission crosstalk may also be high, much higher than in other sensors (e.g., CY-sensor), resulting in the relatively low sensitivity of this probe in our measurement system. Crosstalk effects are undesirable for detection, but it is impossible to completely eliminate these effects in the current measurement system. Maybe we could obtain different results by using spectral imaging in which emission crosstalk is eliminated (12).

According to the characteristics of the fluorescence spectrum, the CY probe seems to be one of the best for FRET-detection. However, the probe is not suitable for imaging with confocal laser microscopy, because the normal argon ion laser, the most common one in confocal microscopes, is not suitable for the excitation of CFP. The blue laser is the most suitable for the excitation, but it is not common in confocal laser microscopes. In this paper, we had to use the argon ion laser emitting 458 nm and the special emission filters optimized for the confocal ratio-imagings of caspase activation using the CY probe (11). On the contrary, the GR probe and the YR probe can be efficiently excited at 488 nm emitted by the normal argon ion laser and imaged with a set of emission filters for fluorescein and a set for rhodamine, with which almost all of the confocal microscopes are equipped. In addition, the GR probe is useful for the detection of caspase activation in flow cytometry, because almost all of the normal flow cytometers are also usually equipped with the laser and the emission filters.

DsRed-containing "red"-sensors have several characteristics that are different from other "non red"-sensors. As previously reported (13), it takes longer for DsRed to mature and emit red fluorescence than it takes for GFPs, and DsRed fluorescence tends to decrease during real-time observation, which may cause a reduction of the apparent sensitivity. These characteristics must be considered when any analysis is performed with these sensors, but as shown in Figs. 4 and 5, red-sensors have a potential similar to that of the CY-sensor and are very useful for multi-color imaging.

It has been reported that DsRed is useful as a fusion tag and a partner for FRET (13, 14). Erickson et al. analyzed the potential of DsRed as a FRET partner with CFP and GFP (14). Mizuno et al. developed a Ca^{2+} sensing fusion protein using Sapphire and DsRed (13). And recently, Karasawa et al. used two novel fluorescent proteins, namely the cyan-emitted and orange-emitted fluorescent proteins from *Acropara* sp. and *Fungia concinna*, respectively, as a FRET pair, and measured caspase-3 activity in cells (15). These results combined with our results indicate that various fluorescent proteins including GFP derivatives, DsRed, and others are useful for FRET analysis. By choosing the appropriate two fluorescent proteins as the FRET pair, we can customize the fluorescent range of FRET-based imaging probes to fit the analysis, which would expand the flexibility of simultaneous multi-event analysis.

By using the CR and YR developed in this study, we were able to analyze two FRET probes simultaneously in the same cells. In several reports, the initiator caspase activity and the effector caspase activity were measured in living cells (8, 9, 11). In these reports, however, each activity was measured independently in different cells. To our knowledge, the present study is the first report that analyzes these activities in the same cell. The results directly reveal the temporal relationships between these caspase activities. It takes a long time for cells to start the initiator caspase activation after drug treatment, but it takes a relatively short time for cells to start the effector caspase activation after the initiator caspase activation. The caspase cascade is initiated at the last stage of cell death signaling, and it proceeds within a short time period.

Acknowledgments

This study was supported in part by a Grant-in-Aid for

Research on Health Sciences Focusing on Drug Innovation from the Japan Health Science Foundation; a Grant-in-Aid for Research on Advanced Medical Technology from the Ministry of Health, Labour, and Welfare; and a grant (MF-16) from the Organization for Pharmaceutical Safety and Research.

References

1 Miyawaki A, Llopis J, Heim R, Mccaffery JM, Adams JA, Ikura M, et al. Fluorescent indicators for Ca^{2+} based on green fluorescent proteins and calmodulin. Nature. 1997;388:882–887.
2 Zaccolo M, Giorgi FD, Cho CY, Feng L, Knapp T, Negulescu PA, et al. A genetically encoded, fluorescent indicator for cyclic AMP in living cells. Nat Cell Biol. 2000;2:25–29.
3 Nagai Y, Miyazaki M, Aoki R, Zama T, Inouye S, Hirose K, et al. A fluorescent indicator for visualizing cAMP-induced phosphorylation in vivo. Nat Biotechnol. 2000;18:313–316.
4 Kurokawa K, Mochizuki N, Ohba Y, Mizuno H, Miyawaki A, Matsuda M. A pair of fluorescent resonance energy transfer-based probes for tyrosine phosphorylation of the CrkII adaptor protein in vivo. J Biol Chem. 2001;276:31305–31310.
5 Sato M, Ozawa T, Inukai K, Asano T, Umezawa Y. Fluorescent indicators for imaging protein phosphorylation in single living cells. Nat Biotechnol. 2002;20:287–294.
6 Tyas L, Brophy VA, Pope A, Rivett AJ, Tavare JM. Rapid caspase-3 activation during apoptosis revealed using fluorescence-resonance energy transfer. EMBO Rep. 2000;1:266–270.
7 Rehm M, Dussmann H, Janicke RU, Tavare JM, Kogel D, Prehn JHM. Single-cell fluorescence resonance energy transfer analysis demonstrates that caspase activation during apoptosis is a rapid process: role of caspase-3. J Biol Chem. 2002;277: 24506–24514.
8 Luo KQ, Yu VC, Pu Y, Chang DC. Measuring dynamics of caspase-8 activation in a single living HeLa cell during TNFα-induced apoptosis. Biochem Biophys Res Commun. 2003;304: 217–222.
9 Takemoto K, Nagai T, Miyawaki A, Miura M. Spatio-temporal activation of caspase revealed by indicator that is insensitive to environmental effects. J Cell Biol. 2003;160:235–243.
10 Tsien RY. The green fluorescent protein. Annu Rev Biochem. 1998;67:509–544.
11 Kawai H, Suzuki T, Kobayashi T, Mizuguchi H, Hayakawa T, Kawanishi T. Simultaneous imaging of initiator/effector caspase activity and mitochondrial membrane potential during cell death in living HeLa cells. Biochim Biophys Acta. 2004;1693:101–110.
12 Zimmermann T, Rietdorf J, Pepperkok R. Spectral imaging and its applications in live cell microscopy. FEBS Lett. 2003;546: 87–92.
13 Mizuno H, Sawano A, Eli P, Hama H, Miyawaki A. Red fluorescent protein from Discosoma as a fusion tag and a partner for fluorescence resonance energy transfer. Biochemistry. 2001; 40:2502–2510.
14 Erickson MG, Moon DL, Yue DT. DsRed as a potential FRET partner with CFP and GFP. Biophys J. 2003;85:599–611.
15 Karasawa S, Araki T, Nagai T, Mizuno H, Miyawaki A. Cyan-emitting and orange-emitting fluorescent proteins as a donor /acceptor pair for fluorescence resonance energy transfer. Biochem J. 2004;381:307–312.

RAPID COMMUNICATIONS IN MASS SPECTROMETRY
Rapid Commun. Mass Spectrom. 2005; **19**: 3315–3321
Published online 31 October 2005 in Wiley InterScience (www.interscience.wiley.com). DOI: 10.1002/rcm.2190

Specific detection of Lewis x-carbohydrates in biological samples using liquid chromatography/multiple-stage tandem mass spectrometry

Noritaka Hashii[1,2], Nana Kawasaki[1,2]*, Satsuki Itoh[1], Akira Harazono[1], Yukari Matsuishi[1,2], Takao Hayakawa[3] and Toru Kawanishi[1]

[1]Division of Biological Chemistry and Biologicals, National Institute of Health Sciences, 1-18-1 Kamiyoga, Setagaya-ku, Tokyo 158-8501, Japan
[2]Core Research for Evolutional Science and Technology (CREST) of Japan Science and Technology Agency (JST), Kawaguchi Center Building, 4-1-8 Hon-cho, Kawaguchi, Saitama 332-0012, Japan
[3]Pharmaceutical and Medical Devices Agency, 3-3-2 Kasumigaseki, Chiyoda-ku, Tokyo 100-0013, Japan

Received 14 July 2005; Revised 5 September 2005; Accepted 8 September 2005

The Lewis x structure [Le^x, Galβ1-4(Fucα1-3)GlcNAc] motif is one of the tumor antigens and plays an important role in oncogenesis, development, cellular differentiation and adhesion. The detection of Le^x-carbohydrates and their structural analysis are necessary to clarify the role of Le^x in several biological events. Mass spectrometry has been preferably used for the structural analysis of carbohydrates. Especially, collision-induced dissociation (CID) tandem mass spectrometry (MS/MS), which causes a glycosidic bond cleavage, is used for carbohydrate sequencing. However, Le^x cannot be identified by MS/MS due to the existence of the positional isomers, such as Lewis a [Galβ1-3(α1-4Fuc)GlcNAc]. In the present study, we demonstrate the specific detection of Le^x-carbohydrates in a biological sample by using multiple-stage MS/MS (MS^n). Using pyridylaminated oligosaccharides bearing Le^x, we found that the Le^x-motif yields a cross-ring fragment by the cleavage of a bond between C-3 and C-4 of GlcNAc in Gal(Fuc)GlcNAc. The Le^x-specific cross-ring fragment ion at *m/z* 259 was effectively detected by sequential scans, consisting of a full MS^1 scan, data-dependent CID MS^2 scan, MS^3 of [Gal(Fuc)GlcNAc+Na]$^+$ at *m/z* 534, and MS^4 of [GalGlcNAc+Na]$^+$ at *m/z* 388. The sequential scan was applied to *N*-linked oligosaccharide profiling using a LC/ESI-MS^n system equipped with a graphitized carbon column. We successfully detected the Le^x-motif and elucidated the structures of several Le^x and Lewis y [(Fucα1-2)Galβ1-4(Fucα1-3)GlcNAc] oligosaccharides in the murine kidney used as a model tissue. Our method is expected to be a powerful tool for the specific detection of the Le^x-motif, and structural elucidation of Le^x-carbohydrates in biological samples. Copyright © 2005 John Wiley & Sons, Ltd.

The Lewis x structure [Le^x, Galβ1-4(Fucα1-3)GlcNAc] is one of the tumor antigens, and plays an important role in oncogenesis[1,2] (abbreviations used here are: Gal, galactose; Fuc, fucose; GlcNAc, *N*-acetylglucosamine). Particularly, sialylated Le^x is used as a marker of lung, pancreas and uterus tumors.[3] Le^x and its derivatives are also known to be oligosaccharide ligands of some endothelial receptors, such as the selectins and the scavenger receptor, C-type lectin,[4,5] and affect embryonic development, cellular differentiation and adhesion.[6,7] However, the structural details of the oligosaccharides attached to the Le^x structure (Le^x-oligosaccharide) are still unclear. Le^x structure-specific detection and elucidation methods are necessary for the diagnosis of tumors and a study on the role of Le^x on various biological events.

Mass spectrometry (MS) has become very popular for the structural analysis of oligosaccharides. Low-energy collision-induced dissociation (CID) tandem mass spectrometry (MS/MS), which generates B/Y-series ions by glycosidic bond cleavage, is preferably used for oligosaccharide sequencing.[8–13] However, the detection of Le^x by MS/MS is still challenging due to the presence of its positional isomer, Lewis a [Le^a, Galβ1-3(Fucα1-4)GlcNAc]. The structural difference between Le^x and Le^a is the linkage at positions 3 or 4 of the non-reducing terminal fucose and galactose to GlcNAc (Fig. 1). For the linkage analysis, multiple-stage MS/MS (MS^n) pattern-matching, in which the oligosaccharide structure can be deduced from intensity ratios of fragment ions generated by MS^n, has recently been reported;[14–16] however, this method needs an identical analytical condition and various oligosaccharide standards. As an alternative method, the cross-ring fragmentation caused by MS^n is

Correspondence to: N. Kawasaki, Division of Biological Chemistry and Biologicals, National Institute of Health Sciences, 1-18-1 Kamiyoga, Setagaya-ku, Tokyo 158-8501, Japan.
E-mail: nana@nihs.go.jp
Contract/grant sponsor: Ministry of Health Labor and Welfare, and Core Research for the Evolutional Science and Technology Program, Japan Science and Technology Corp.

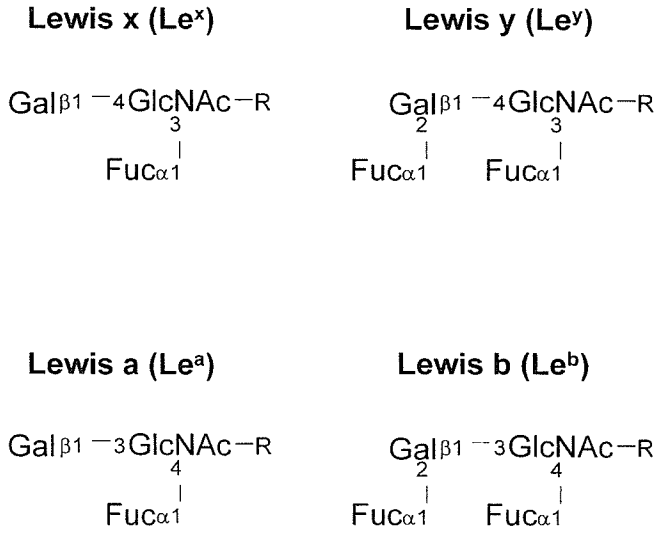

Figure 1. Structures of Lewis a, b, x and y.

sometimes used.[10,17,18] Meisen *et al.*[19] demonstrated that α2-6-linked *N*-acetylneuraminic acid (NeuNAc) can be distinguished from α2-3-linked NeuNAc based on structure-specific cross-ring fragment ions generated by low-energy CID MS^2 in the negative ion mode. Le^x could be expected to be distinguished from its positional isomers by cross-ring fragmentation.

In this study, we demonstrate the specific detection of Le^x-carbohydrates in a biological sample by using MS^n. Using pyridylaminated oligosaccharides bearing Le^x, we found that the Le^x-motif yields a cross-ring fragment by the cleavage of a bond between C-3 and C-4 of GlcNAc in Gal(Fuc)GlcNAc. The Le^x-specific cross-ring fragment ion at *m/z* 259 was effectively detected by sequential scans, consisting of a full MS^1 scan, data-dependent CID MS^2 scan, MS^3 of $[Gal(Fuc)GlcNAc+Na]^+$ at *m/z* 534, and MS^4 of $[GalGlcNAc+Na]^+$ at *m/z* 388 using nano-electrospray ionization-ion trap mass spectrometry (nanoESI-ITMS) in positive ion mode. Then, sequential MS^{1-4} scanning for the Le^x-characteristic ions was applied for *N*-linked oligosaccharide profiling using an LC/ESI-ITMS instrument equipped with a graphitized carbon column (GCC), by which diverse oligosaccharides, including isomers, can be separated. We successfully detected the Le^x-motif and subsequently elucidated the entire structure of Le^x-oligosaccharides in the model tissue, murine kidney, in which Le^x-oligosaccharides are abundantly present.[20]

EXPERIMENTAL

Materials

2-Aminopyridine (PA)-labeled pentasaccharides bearing Le^x (oligosaccharide I, Fig. 2(A)) or Le^a (oligosaccharide II, Fig. 2(B)), and the asialotriantennary oligosaccharide bearing Le^x (oligosaccharide III, Fig. 2(C)), were purchased from Takara Biomedicals (Otsu, Japan). Murine kidneys (MRL/MpJ-+/+) were purchased from Japan SLC Inc. (Hamamatsu, Japan).

Sample preparation

Proteins from murine kidneys were solubilized in lysis buffer (7 M urea, 2 M thiourea, 2% CHAPS, 30 mM Tris-HCl) by vortexing at room temperature. The proteins (100 μg) were recovered by precipitation in cold acetone, and then treated with 10 units of PNGase F in 500 μL of 0.2 M phosphate buffer (pH 7.6) at 37°C for 48 h to release the *N*-linked oligosaccharides. Proteins were removed by precipitation in cold ethanol, and the supernatant containing oligosaccharides was evaporated and lyophilized. The dried oligosaccharides were labeled with PA according to a previous report.[21] The PA-labeled oligosaccharides were desalted with Envi-Carb C (Supelco Bellefonte, USA) and lyophilized.

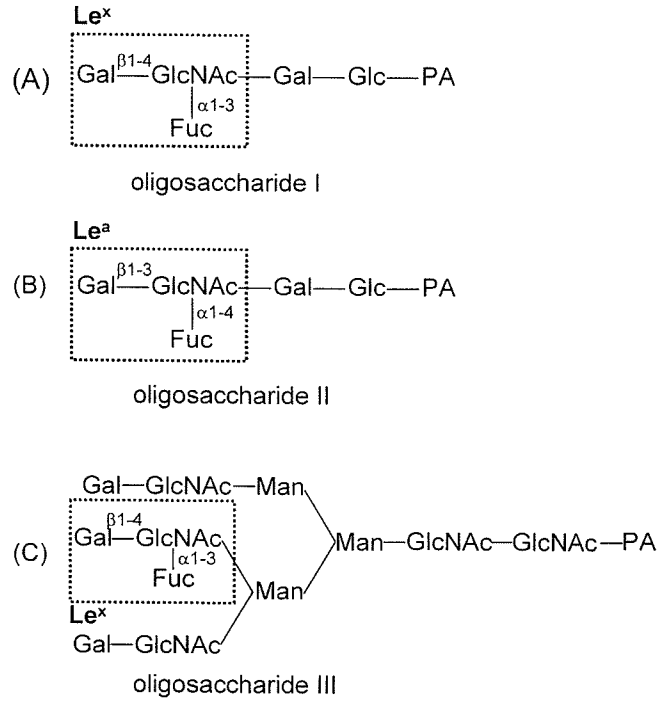

Figure 2. Structures of model oligosaccharides used in this study: (A) PA-labeled Le^x-pentasaccharide (oligosaccharide I); (B) PA-labeled Le^a-pentasaccharide (oligosaccharide II); and (C) PA-labeled Le^x-asialotriantennary complex type oligosaccharide (oligosaccharide III).

nanoESI-MS^n

Experiments were performed using a Finnigan linear ion trap Fourier transform ion cyclotron resonance mass spectrometer (LTQ-FT, ThermoElectron, San Jose, CA, USA) equipped with a nanoESI source (AMR, Inc., Tokyo, Japan). ESI-MS^n was carried out for Le^x- and Le^a-oligosaccharide standards at a concentration of 1 pmol/μL in 5 mM ammonium acetate and 10 μM NaCl buffer (pH 9.6) containing 50% acetonitrile. The sample was analyzed at a flow rate of 2.0 μL/min using a spray voltage of 2.0 kV in the positive ion mode. The capillary temperature was set to 200°C; collision energies were set to 20–30% for the MS^n experiments; the maximum scan time was set to 50 ms. MS^2 and MS^3 were performed with an isolation width of 3.0 u (range of precursor ion ±1.5).

LC/MS^n

LC was carried out using a MAGIC 2002 system (Michrom BioResources, Auburn, CA, USA) equipped with a GCC (Hypercarb column, 150 × 0.2 mm, ThermoElectron). The

eluents were 5 mM ammonium acetate, pH 9.6, containing 2% acetonitrile (pump A) and 5 mM ammonium acetate, pH 9.6, containing 80% acetonitrile (pump B). PA-labeled *N*-linked oligosaccharides from murine kidney were eluted at a flow rate of 2 μL/min with a gradient of 10–70% of pump B in 60 min. A solution of NaCl (10 μM) was passed post-column at a flow rate of 2 μL/min. The precursor ions detected by a full MS^1 scan (mass range at *m/z* 750–2000) were followed by MS^2 scans of the most intense ions.

RESULTS AND DISCUSSION

MS^n of Le^x-pentaoligosaccharide

The model Le^x-pentaoligosaccharide (oligosaccharide I) was analyzed by nanoESI-MS^n with direct injection in the positive ion mode. Sodium chloride (NaCl) was deliberately added to the sample for the acceleration of the cross-ring cleavages according to previous reports.[22–24] The sodiated singly charged molecular ion, $[M+Na]^+$, of oligosaccharide I was observed at *m/z* 954.4 in the MS^1 spectrum (Fig. 3(A)). MS^2 of the sodiated molecular ion yielded $[(M+Na)\text{-Fuc}]^+$ at *m/z* 808 as the most intense ion by the glycosidic bond cleavage between GlcNAc and Fuc residues (Fig. 3(B)). This indicates that the Fuc residue is easily dissociated by low-energy CID MS^2. In addition to the defucosylated ions, we observed the sodiated ion at *m/z* 534, corresponding to the Le^x and Le^a structure, $[Gal(Fuc)GlcNAc+Na]^+$. The sodiated B_2 ion (*m/z* 534) was subjected to a further product ion scan, and the sodiated ion at *m/z* 388 corresponding to $[GalGlcNAc+Na]^+$ appeared in the MS^3 spectrum (Fig. 3(C)). The ion at *m/z* 372, corresponding to $[FucGlcNAc+Na]^+$, which proves the attachment of Fuc to GlcNAc, was also detected. Then, MS^4 of the sodiated $Y_{3\alpha}$ ion (*m/z* 388) yielded a sodiated cross-ring fragment ion at *m/z* 259, corresponding to the sodiated $^{3,5}A_2$ ion, which proves the linkage of the Gal residue at position C-4 on GlcNAc, with some neutral losses: 60 Da ($^{0,4}A_2$, $^{0,4}X_{4\beta}$, $^{1,3}X_{4\beta}$ and $^{2,4}X_{4\beta}$) and 90 Da ($^{0,3}X_{4\beta}$ and $^{1,4}X_{4\beta}$) (Fig. 3(D)).

MS^n of Le^a-pentaoligosaccharide

The Le^a-pentasaccharide (oligosaccharide II) was subjected to nanoESI-MS^n in a similar manner. The $[M+Na]^+$ of oligosaccharide II was observed at *m/z* 954.4 in the MS^1 spectrum (Fig. 4(A)). MS^2 of the $[M+Na]^+$ at *m/z* 954 yielded the sodiated ion at *m/z* 534, corresponding to $[Gal(Fuc)GlcNAc+Na]^+$ (Fig. 4(B)). MS^3 of the sodiated B_2 ion (*m/z* 534) yielded the sodiated $Y_{3\alpha}$ and $Y_{3\beta}$ ions at *m/z* 372 and 388, respectively (Fig. 4(C)). MS^4 of the sodiated $Y_{3\beta}$ ion at *m/z* 388 yielded some cross-ring fragment ions at *m/z* 208, 268, 298 and 328, corresponding to neutral losses: 60 Da ($^{0,4}A_2$, $^{0,4}X_{4\beta}$, $^{1,3}X_{4\beta}$ and $^{2,4}X_{4\beta}$) and 90 Da ($^{0,3}A_2$, $^{0,3}X_{4\beta}$ and $^{1,4}X_{4\beta}$) (Fig. 4(D)). $^{3,5}A_2$ at *m/z* 259, which arose from oligosaccharide I, was not detected by MS^4 of Le^a.

These results suggest that the Le^x structure can be identified by the $^{3,5}A_2$ ion at *m/z* 259 generated by MS^4 of $[GalGlcNAc+Na]^+$ at *m/z* 388, which arose from MS^3 $[Gal(Fuc)GlcNAc+Na]^+$ at *m/z* 534 (Fig. 5).

MS^n of Le^x-asialotriantennary oligosaccharide

Using a Le^x-oligosaccharide with a more complicated branching structure, we confirmed the practicability of MS^3 of the ion at *m/z* 534 followed by MS^4 of the ion at *m/z* 388 for the detection of the Le^x-diagnostic ion at *m/z* 259.

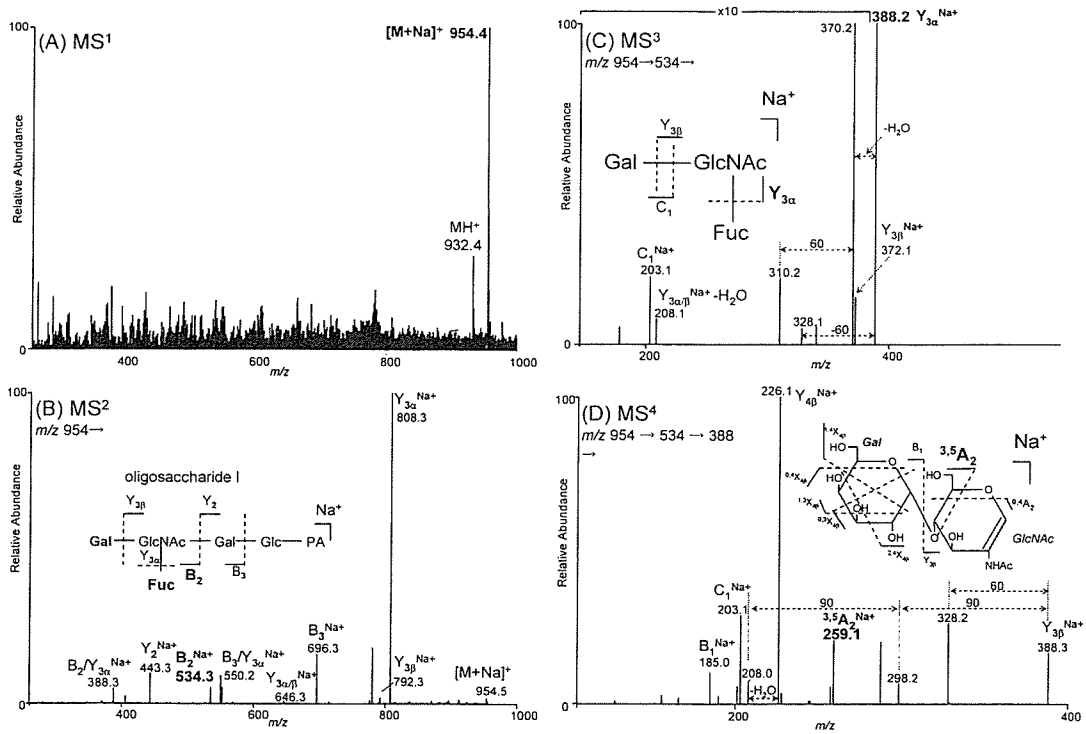

Figure 3. MS$^{1-4}$ spectra of oligosaccharide I by ESI-MS^n: (A) MS^1 spectrum; (B) MS^2 spectrum of $[M+Na]^+$ at *m/z* 954.4; (C) MS^3 spectrum of $[Gal(Fuc)GlcNAc+Na]^+$ at *m/z* 534.3 detected in MS^2; and (D) MS^4 spectrum of $[GalGlcNAc+Na]^+$ at *m/z* 388.2 detected in MS^3.

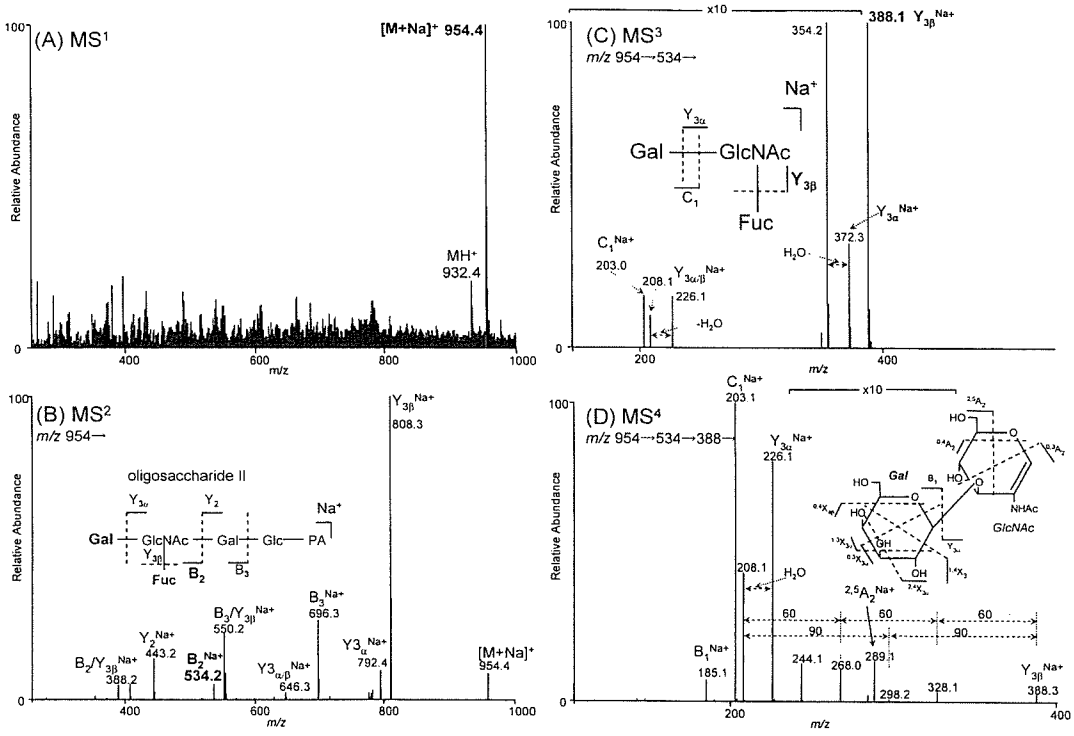

Figure 4. MS^{1-4} spectra of oligosaccharide II by ESI-MS^n: (A) MS^1 spectrum; (B) MS^2 spectrum of $[M+Na]^+$ at *m/z* 954.4; (C) MS^3 spectrum of $[Gal(Fuc)GlcNAc+Na]^+$ at *m/z* 534.2 detected in MS^2; and (D) MS^4 spectrum of $[GalGlcNAc+Na]^+$ at *m/z* 388.1 detected in MS^3.

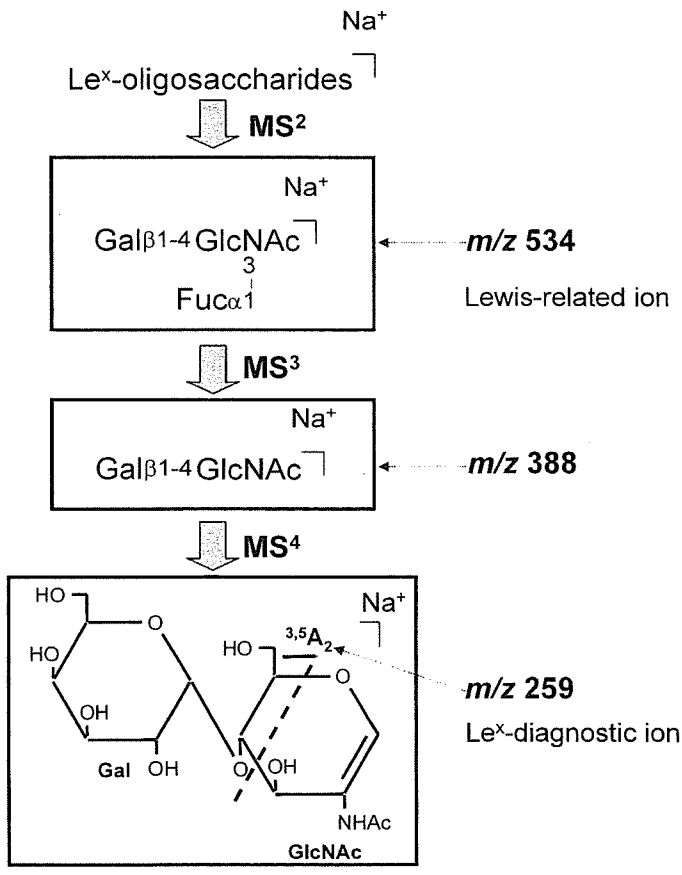

Figure 5. Proposed method for the Le^x-specific detection by ESI-MS^n.

Figure 6 shows the MS^{2-4} spectra of Le^x-asialotriantennary (oligosaccharide III). The oligosaccharide sequence can be confirmed by product ions generated by MS^2 (Fig. 6(A)). In addition to the defucosylated ion, many B- and Y-series ions, including the sodiated ion at *m/z* 534 corresponding to $[Gal(Fuc)GlcNAc+Na]^+$, were generated by MS^2. MS^3 of the sodiated $B_{2\alpha'}$ ion at *m/z* 534 yielded the sodiated $Y_{5\alpha''}$ ion at *m/z* 388 as the most intense ion (Fig. 6(B)). MS^4 of the $Y_{5\alpha''}$ ion at *m/z* 388 predictably generated the $^{3,5}A_2$ ion (*m/z* 259) (Fig. 6(C)). These results indicate that MS^3 of the sodiated ion at *m/z* 534, followed by MS^4 of the sodiated ion at *m/z* 388, can be used for the detection of the Le^x-diagnostic motif even in large and complicated *N*-linked oligosaccharides.

Specific detection and structural elucidation of *N*-linked Le^x-oligosaccharides in murine kidney by LC/ESI-MS^n

A sequential scan consisting of a full MS^1 scan, data-dependent MS^2 scan, MS^3 scan of the ion at *m/z* 534, and MS^4 scan of the ion at *m/z* 388 was applied to the specific detection and structural elucidation of Le^x-oligosaccharides in the murine kidney. In order to separate the many different oligosaccharides, including isomers, we used a LC/ITMS system equipped with a GCC. The *N*-linked oligosaccharides were released by PNGase F from the carboxymethylated proteins in the murine kidney soluble fraction. To improve the ionization efficiency and sensitivity,[25,26] the oligosaccharides were pyridylaminated, and the PA-oligosaccharides were subjected to LC/ESI-MS^n with a sequential scan. Sodiated ions were generated by a post-column reaction with 10 μM NaCl solution (2 μL/min). Oligosaccharides that yielded the

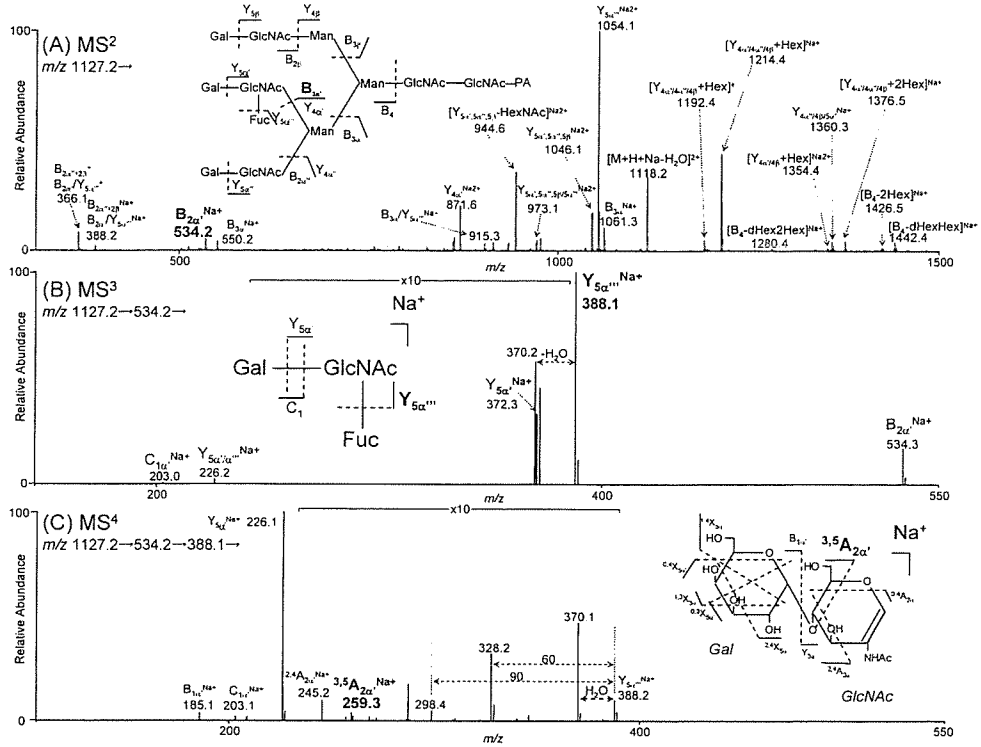

Figure 6. MS$^{2-4}$ spectra of oligosaccharide III by ESI-MS^n: (A) MS^2 spectrum of $[M+H+Na]^{2+}$ at *m/z* 1127.2; (B) MS^3 spectrum of $[Gal(Fuc)GlcNAc+Na]^+$ at *m/z* 534.2 detected in MS^2; and (C) MS^4 spectrum of $[GalGlcNAc+Na]^+$ at *m/z* 388.1 detected in MS^3.

diagnostic ions by MS$^{1-4}$ scans were presumed to be those of Le^x-oligosaccharides, and their detailed structures were elucidated by their data-dependent MS^2 spectra.

Figure 7(A) shows the total ion current (TIC) profile obtained by the full MS^1 scan of PA-labeled oligosaccharides from the murine kidney. Structures of major oligosaccharides a–i were deduced from the masses of the sodiated molecular ions measured by FTMS together with the B/Y ions generated by CID MS^2 (Table 1). Figures 7(B)–7(D) show mass chromatograms at *m/z* 534, 388 and 259, respectively, detected by MS$^{2-4}$, respectively. These chromatograms revealed that at least five kinds of oligosaccharides contain the Le^x-motif (a, b, e, f and h). Based on the masses, they were assigned to fucosylated oligosaccharides consisting of $dHex_3Hex_5HexNAc_5$ (a and f), $dHex_2Hex_5HexNAc_5$ (b), $dHexHex_4HexNAc_5$ (e), and $dHex_2Hex_4HexNAc_5$ (h) (abbreviations used here are: dHex, deoxyhexose; Hex, hexose; HexNAc, *N*-acetylhexosamine).

As an example of structural elucidation, we show the MS$^{2-4}$ spectra of oligosaccharide f in Fig. 8. In the MS^2 spectrum, we can observe the product ion $[dHex_2HexHexNAc+Na]^+$ at *m/z* 680, which can be assigned to either the Lewis b (Le^b)- or Lewis y (Le^y)-motif. As shown in Fig. 1, Le^b- and Le^y-motifs contain Le^a and Le^x as partial structures, respectively. The generation of Le^x-diagnostic ions suggests the attachment of the Le^y-motif to oligosaccharide f. Furthermore, product ions at *m/z* 1036 and 446 prove the linkage of GlcNAc at β-mannose in the trimannosyl core structure and fucosylation of the reducing terminal GlcNAc, respectively. Based on these characteristic ions, oligosaccharide f can be assigned to the bisected and fucosylated biantennary bearing the

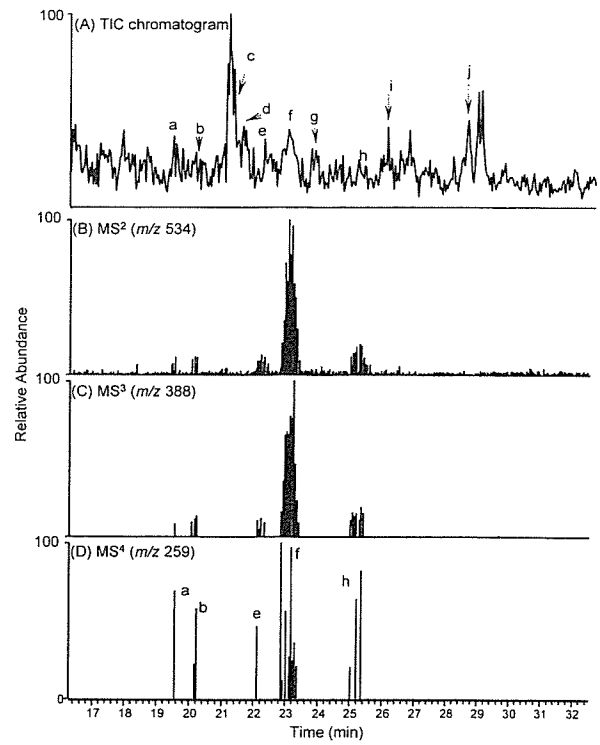

Figure 7. Specific detection of *N*-linked Le^x-oligosaccharides in murine kidney by LC/ESI-MS^n: (A) total ion chromatogram obtained by MS^1; (B) mass chromatogram of $[dHexHexNAc+Na]^+$ at *m/z* 534 detected in MS^2; (C) mass chromatogram of $[HexHexNAc+Na]^+$ at *m/z* 388 detected in MS^3; and (D) mass chromatogram of the cross-ring fragment at *m/z* 259 detected in MS^4.

RCM

Table 1. Sugar composition and deduced structure of *N*-linked oligosaccharide from murine kidney

Sugar No.	Composition[a]	Deduced structure	Lewis type
a	$dHex_3Hex_5HexNAc_5$	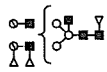	Le^y
b	$dHex_2Hex_5HexNAc_5$	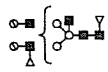	Le^x
c	$Hex_8HexNAc_2$	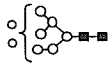	
d	$Hex_9HexNAc_2$		
e	$dHexHex_4HexNAc_5$	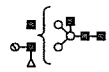	Le^x
f	$dHex_3Hex_5HexNAc_5$	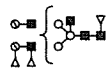	Le^y
g	$Hex_6HexNAc_2$		
h	$dHex_2Hex_4HexNAc_5$		Le^x
i	$Hex_7HexNAc_2$	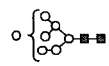	
j	$Hex_5HexNAc_2$		

[a]Fuc, fucose; Hex, hexose; HexNAc, *N*-acetylhexosamine.
○ Gal; ○ Man; ■ GlcNAc; △ Fuc.

Le^y-motif. The Le^y structure in oligosaccharide f was confirmed by an extra LC/MS^2 run without post-column reaction with NaCl. Figure 9 shows the MS^2 spectrum of $[M+H+NH_4]^{2+}$ at *m/z* 1189.4. Attachment of the Le^y-motif was proved by the generation of the product ion at *m/z* 658 corresponding to $[dHex_2HexHexNAc]^+$.

Other oligosaccharides were assigned to bisected biantennary forms bearing Le^y (oligosaccharide a) and those bearing Le^x (oligosaccharides b, e and h) motifs. In addition to the previously reported Le^x-oligosaccharides,[20] we also detected the presence of Le^y-oligosaccharides in the murine kidney.

CONCLUSIONS

We found that the cross-ring fragment ion at *m/z* 259, which can be used for distinction from positional isomers, was generated from Le^x-oligosaccharides by MS^4 of $[GalGlcNAc+Na]^+$ at *m/z* 388, which was generated by MS^3 of $[Gal(Fuc)GlcNAc+Na]^+$ at *m/z* 534. Then, we successfully detected and elucidated the Le^x- and Le^y-oligosaccharides in the complex mixture using a sequential scan consisting of full MS^1, data-dependent MS^2, MS^3 of the sodiated ion at *m/z* 534, and MS^4 of the sodiated ion at *m/z* 388.

The Le^x structure is associated with various biological events as oligosaccharide ligands. So far, the detection and structural analyses of Le^x-oligosaccharides have required complicated and time-consuming processes, such as exoglycosidase digestions, sugar mapping,[27] the use of lectins and immunological methods. The mass spectrometric method proposed here would enable the rapid and easy detection of the Le^x-motif and subsequent structural elucidation of

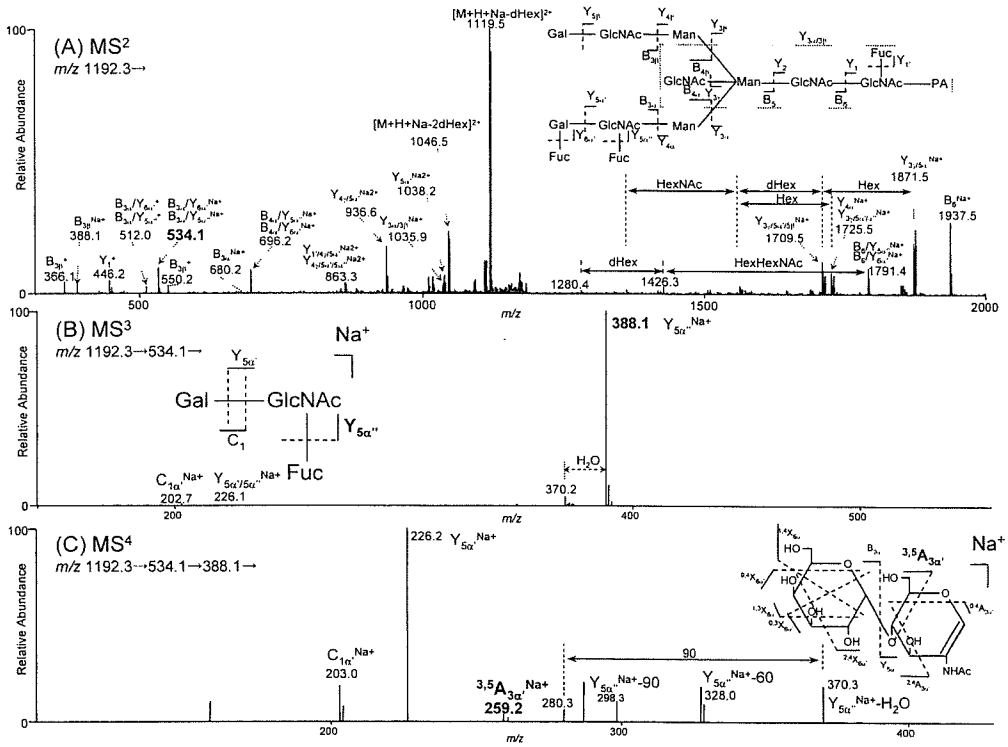

Figure 8. MS^{2-4} spectra of oligosaccharide f by LC/ESI-MS^n: (A) MS^2 spectrum of $[M+H+Na]^{2+}$ at *m/z* 1192.3; (B) MS^3 spectrum of $[dHexHexNAc+Na]^+$ at *m/z* 534.1 detected in MS^2; and (C) MS^4 spectrum of $[HexHexNAc+Na]^+$ at *m/z* 388.1 detected in MS^3.

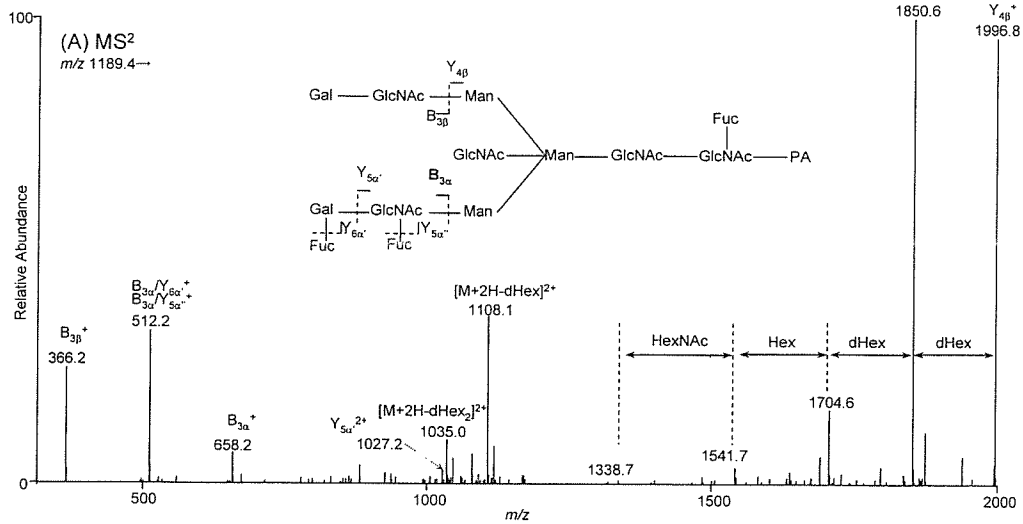

Figure 9. MS^2 spectrum of oligosaccharide f by LC/ESI-MS^n: precursor ion, $[M+H+NH_4]^{2+}$ at *m/z* 1189.9.

Le^x-oligosaccharides in biological samples. Our method, based on a sequential scan for the structure-characteristic ions, may be applicable to the analyses of oligosaccharides carrying other partial motifs, such as sialyl Le^x and sulfated sugar.

Acknowledgements

This study was supported in part by Grant-in-Aid from the Ministry of Health Labor and Welfare, and Core Research for the Evolutional Science and Technology Program, Japan Science and Technology Corp.

REFERENCES

1. Feizi T. *Nature* 1985; **314**: 53.
2. Walz G, Aruffo A, Kolanus W, Bevilacqua M, Seed B. *Science* 1990; **250**: 1132.
3. Kannagi R, Izawa M, Koike T, Miyazaki K, Kimura N. *Cancer Sci.* 2004; **95**: 377.
4. Coombs PJ, Graham SA, Drickamer K, Taylor ME. *J. Biol. Chem.* 2005; **280**: 22993.
5. Larkin M, Ahern TJ, Stoll MS, *et al. J. Biol Chem.* 1992; **267**: 13661.
6. Lowe JB, Stoolman LM, Nair RP, Larsen RD, Berhend TL, Marks RM. *Cell* 1990; **63**: 475.
7. Phillips ML, Nudelman E, Gaeta FC, Perez M, Singhal AK, Hakomori S, Paulson JC. *Science* 1990; **250**: 1130.
8. Sagi D, Peter-Katalinic J, Conradt HS, Nimtz M. *J. Am. Soc. Mass Spectrom.* 2002; **13**: 1138.
9. Sheeley DM, Reinhold VN. *Anal. Chem.* 1998; **70**: 3053.
10. Xue J, Song L, Khaja SD, Locke RD, West CM, Laine RA, Matta KL. *Rapid Commun. Mass Spectrom.* 2004; **18**: 1947.
11. Karlsson NG, Schulz BL, Packer NH. *J. Am. Soc. Mass Spectrom.* 2004; **15**: 659.
12. Karlsson NG, Wilson NL, Wirth HJ, Dawes P, Joshi H, Packer NH. *Rapid Commun. Mass Spectrom.* 2004; **18**: 2282.
13. Zhang S, Chelius D. *J. Biomol. Technol.* 2004; **15**: 120.
14. Royle L, Mattu TS, Hart E, Langridge JI, Merry AH, Murphy N, Harvey DJ, Dwek RA, Rudd PM. *Anal. Biochem.* 2002; **304**: 70.
15. Takegawa Y, Deguchi K, Ito S, Yoshioka S, Nakagawa H, Nishimura S. *Rapid Commun. Mass Spectrom.* 2005; **19**: 937.
16. Takegawa Y, Ito S, Yoshioka S, Deguchi K, Nakagawa H, Monde K, Nishimura S. *Rapid Commun. Mass Spectrom.* 2004; **18**: 385.
17. Mechref Y, Novotny MV, Krishnan C. *Anal Chem.* 2003; **75**: 4895.
18. Weiskopf AS, Vouros P, Harvey DJ. *Anal. Chem.* 1998; **70**: 4441.
19. Meisen I, Peter-Katalinic J, Muthing J. *Anal. Chem.* 2003; **75**: 5719.
20. Chui D, Sellakumar G, Green R, Sutton-Smith M, McQuistan T, Marek K, Morris H, Dell A, Marth J. *Proc. Natl. Acad. Sci. USA* 2001; **98**: 1142.
21. Yuan J, Hashii N, Kawasaki N, Itoh S, Kawanishi T, Hayakawa T. *J. Chromatogr. A* 2005; **1067**: 145.
22. Song F, Cui M, Liu Z, Yu B, Liu S. *Rapid Commun. Mass Spectrom.* 2004; **18**: 2241.
23. Cui M, Song F, Liu Z, Liu S. *Rapid Commun. Mass Spectrom.* 2001; **15**: 586.
24. Vakhrushev SY, Zamfir A, Peter-Katalinic J. *J. Am. Soc. Mass Spectrom.* 2004; **15**: 1863.
25. Suzuki S, Kakehi K, Honda S. *Anal. Chem.* 1996; **68**: 2073.
26. Yoshino K, Takao T, Murata H, Shimonishi Y. *Anal. Chem.* 1995; **67**: 4028.
27. Tomiya N, Awaya J, Kurono M, Endo S, Arata Y, Takahashi N. *Anal Biochem.* 1988; **171**: 73.

Available online at www.sciencedirect.com
SCIENCE DIRECT
ELSEVIER
Journal of Chromatography A, 1094 (2005) 105–117
JOURNAL OF CHROMATOGRAPHY A
www.elsevier.com/locate/chroma

Characterization of a gel-separated unknown glycoprotein by liquid chromatography/multistage tandem mass spectrometry Analysis of rat brain Thy-1 separated by sodium dodecyl sulfate-polyacrylamide gel electrophoresis

Satsuki Itoh [a], Nana Kawasaki [a,b,*], Akira Harazono [a], Noritaka Hashii [a], Yukari Matsuishi [b], Toru Kawanishi [a], Takao Hayakawa [a]

[a] *Division of Biological Chemistry and Biologicals, National Institute of Health Science, 1-18-1, Kamiyoga, Setagaya-ku, Tokyo 158-8501, Japan*
[b] *CREST, Japan Science and Technology Agency (JST), Japan*

Received 17 May 2005; received in revised form 17 July 2005; accepted 25 July 2005
Available online 5 October 2005

Abstract

We developed an efficient and convenient strategy for protein identification and glycosylation analysis of a small amount of unknown glycoprotein in a biological sample. The procedure involves isolation of proteins by electrophoresis and mass spectrometric peptide/glycopeptide mapping by LC/ion trap mass spectrometer. For the complete glycosylation analysis, proteins were extracted in intact form from the gel, and proteinase-digested glycoproteins were then subjected to LC/multistage tandem MS (MS^n) incorporating a full mass scan, in-source collision-induced dissociation (CID), and data-dependent MS^n. The glycopeptides were localized in the peptide/glycopeptide map by using oxonium ions such as $HexNAc^+$ and $NeuAc^+$, generated by in-source CID, and neutral loss by CID-MS/MS. We conducted the search analysis for the glycopeptide identification using search parameters containing a possible glycosylation at the Asn residue with *N*-acetylglucosamine (203 Da). We were able to identify the glycopeptides resulting from predictable digestion with proteinase. The glycopeptides caused by irregular cleavages were not identified by the database search analysis, but their elution positions were localized using oxonium ions produced by in-source CID, and neutral loss by the data-dependent MS^n. Then, all glycopeptides could be identified based on the product ion spectra which were sorted from data-dependent CID-MS^n spectra acquired around localized positions. Using this strategy, we successfully elucidated site-specific glycosylation of Thy-1, glycosylphosphatidylinositol (GPI)-anchored proteins glycosylated at Asn23, 74, and 98, and at Cys111. High-mannose-type, complex-type, and hybrid-type oligosaccharides were all found to be attached to Asn23, 74 and 98, and four GPI structures could be characterized. Our method is simple, rapid and useful for the characterization of unknown glycoproteins in a complex mixture of proteins.

Keywords: Glycoprotein; LC/MS; Ion trap mass spectrometer; In-source CID; Thy-1

1. Introduction

Glycosylation is one of the most abundant post-translational modifications of proteins [1]. Most glycoproteins exist in heterogeneous forms due to their carbohydrate heterogeneity at multiple glycosylation sites. Because heterogeneity at each glycosylation site can be associated with many biological functions [2,3], it is necessary to analyze the oligosaccharide structures at each glycosylation site.

Mass spectrometric peptide/glycopeptide mapping by liquid chromatography coupled with electrospray ionaization tandem mass spectrometry (LC/ESI-MS/MS) is now used for characterization of glycoproteins [4,5]. Site-specific glycosylation of some gel-separated glycoproteins can be analyzed by in-gel proteinase digestion followed by MS; this method, however, gives unsatisfactory results due to a lower recovery of some glycopeptides from the gel [6–8]. For

* Corresponding author. Tel.: +81 3 3700 1141; fax: +81 3 3707 6950.
E-mail address: nana@nihs.go.jp (N. Kawasaki).

0021-9673/$ – see front matter © 2005 Elsevier B.V. All rights reserved.
doi:10.1016/j.chroma.2005.07.100

complete site-specific glycosylation analysis, all glycopeptide fragments should be recovered from the gel. Hence, the extraction of a whole glycoprotein from the gel before proteinase digestion would be more reasonable than in-gel digestion. Additionally, the poor ionization efficiency of glycopeptides makes it difficult to analyze the glycosylation of glycopeptides in a complex mixture of peptides [6,9]. The glycopeptide-specific method is required for mass spectrometric peptide/glycopeptide mapping.

A precursor ion scan using triple quadrupole-type mass spectrometer is favorably used for analysis of glycopeptides [10–13]. However, this method requires repetitive analysis for the protein identification and glycosylation analysis, as it monitors carbohydrate marker ions such as $HexNAc^+$ and $Hex\text{-}HexNAc^+$ fragmented from glycopeptides by collision-induced dissociation (CID)-MS/MS, and does not provide product ion spectra of non-glycosylated peptides. As such, additional analysis would not be possible for small quantities of proteins, including gel-separated glycoproteins. As an alternative method, we have previously demonstrated peptide/glycopeptide mapping using quadrupole time-of-flight mass spectrometer, by which product ions arise from both peptides and carbohydrates [14]. Using oxonium ions as marker ions, we can sort out product ion spectra of glycopeptides from a number of product ion spectra of peptides, and can determine the amino acid sequences of glycopeptides, glycosylation sites, and monosaccharide composition in a single analysis. Recently, ion trap mass spectrometry (ITMS), which is capable of data-dependent multistage tandem MS (MS^n), has been found to be preferable for use in glycosylation analysis of glycopeptides [15,16]. Glycopeptide-specific detection by precursor ion scan and data-dependent scan cannot be used for glycosylation analysis by ITMS due to the low mass cut-off system. Instead, oxonium ions fragmented by in-source CID are used for the localization of glycopeptides in the peptide/glycopeptide map [3,17]. It has recently been reported that peptide + GlcNAc ions originating from *N*-glycosylated peptides by MS^2 yield peptide b and y ions by further MS^n, and that the peptide sequence and *N*-glycosylation sites can be identified based on the peptide fragment ions [15,16,18]. In addition, another group has reported that glycopeptides can be identified in peptide/glycopeptide map by a search analysis using a database to which all possible cleavage products of the glycopeptides have been added in advance [19]. A combination of peptide/glycopeptide mapping with in-source CID, data-dependent CID-MS^n, and the database search analysis would enable protein identification, glycopeptide selection, and glycosylation analysis of a small amount of glycoprotein.

In the present study, we developed a strategy for the characterization of a small amount of unknown glycoprotein in a biological sample. An unknown glycoprotein was isolated by electrophoresis and extracted from the gel in an intact form. We used sodium dodecyl sulfate (SDS), which is effective for extracting proteins from the gel, and could be easily removed by adding cold acetone. The proteinase-digested glycoprotein was subjected to peptide/glycopeptide mapping, with the sequential scan consisting of a full mass scan, in-source CID, and data-dependent CID-MS^n. Using this method, we carried out site-specific glycosylation analysis of glycosylphosphatidylinositol (GPI)-anchored proteins in rat brain. A computer database search was used for the identification of a GPI-anchored protein and its *N*-glycosylation sites. In-source CID and data-dependent CID-MS/MS were also used for localization of peptides with *N*-glycan and GPI in the peptide/glycopeptide map. On the basis of their product ion spectra, we elucidated *N*-glycosylation at each glycosylation site and the structure of GPIs.

2. Experimental

2.1. Materials

Rat brains were purchased from Nippon SLC (Hamamatsu, Japan). Trypsin-Gold and endoproteinase Asp-N were purchased from Promega (Madison, WI, USA) and Wako Pure Chemical (Osaka, Japan), respectively. Phosphatidylinositol-specific phospholipase C (PIPLC) from *Bacillus cereus* were purchased from Molecular Probes (Eugene, OR, USA). All other chemicals used were of the highest purity available.

2.2. Sodium dodecyl sulfate-polyacrylamide gel electrophoresis (SDS-PAGE) of PIPLC-treated GPI-anchored proteins

PIPLC-treated GPI-anchored proteins were prepared from rat brain utilizing Triton X-114 phase partition and PIPLC digestion [20,21]. Two whole rat brains (2.8 g, Wistar, male, 3 weeks) were homogenized in cold acetone and centrifuged for 10 min at 4 °C. The precipitate was then homogenized in $CHCl_3$: methanol (2:1, v/v) and centrifuged for 10 min at 4 °C. After being washed with methanol, the pellet was homogenized in 50 mM Tris–HCl (pH 7.4) containing 150 mM NaCl, 1 mM ethylenediaminetetraacetic acid (EDTA), and 1 mM phenylmethylsulfonyl fluoride (PMSF), and centrifuged at 10,000 × *g* at 4 °C for 20 min. The pellet was resuspended in the same buffer with an additional 2% Triton X-114 (v/v), and stirred at 4 °C for 16 h. After centrifugation at 10,000 × *g* at 4 °C for 20 min, the supernatant was subjected to Triton X-114 phase-partitioning at 37 °C for 10 min. The detergent phase was resuspended with an equal volume of 50 mM Tris–HCl (pH 7.4) containing 150 mM NaCl. Solubilized membrane proteins in the detergent phase were precipitated with cold acetone and were resuspended in 400 μl of 50 mM Tris–HCl (pH 7.4). Following the addition of PIPLC (1 U), the suspension was incubated at 37 °C for 18 h. The suspension was resubjected to Triton X-114 phase-partitioning, and PIPLC-treated GPI-anchored proteins were precipitated with cold acetone from the aqueous phase. PIPLC-treated GPI-anchored proteins obtained from

50 mg of rat brain were separated by SDS-PAGE (12.5%) after carboxyamidomethylation [22].

2.3. Extraction and digestion of gel-separated proteins

The protein in gel band was extracted with 20 mM Tris–HCl containing 1% SDS by shaking vigorously overnight after breaking down the gel into small bits. The extract was filtered with Ultrafree-MC (0.22 μm, Millipore, Bedford, USA), and the protein was precipitated by adding cold acetone. The precipitate was digested with trypsin (1 μg) in 20 μl of 0.1 M Tris–HCl (pH8.0) at 37 °C for 16 h, or with Asp-N (0.4 μg) in 20 μl of 5 mM Tris–HCl (pH 7.5) at 37 °C overnight.

2.4. LC/MS^n

Proteolytic peptides were separated by a Magic C18 column (50 mm × 0.2 mm, 3 μm, Michrom BioResources, Auburn, CA, USA) with a Paradaim MS4 HPLC system (Michrom BioResources Inc., Auburn, CA, USA) consisting of pump A: 0.1% formic acid and 2% acetonitrile, and pump B: 0.1% formic acid and 90% acetonitrile. Separation was performed with a linear gradient of 5–65% of pump B in 40 min after 5% in 10 min of pump B at a flow rate 3 μl/min. Mass spectra were recorded by Finnigan LTQ (Thermo Electron, San Jose, CA, USA) with the sequential scan: a full mass scan (m/z 300–2000), a full mass scan with in-source CID (m/z 80–500, collision energy: 50 V), and data-dependent CID-MS^n for most intense ions at each scan with dynamic exclusion for 30 s. Scan time (m/z 300–2000) is approximately 0.1 s. The operating condition used for LC/ITMS was as follows: tube lens offset of 130 V, capillary voltage of 2.0 kV, capillary temperature of 200 °C.

2.5. Computer database search analysis

All product ions obtained by LC/ITMS were subjected to the computer database search analysis with the TurboSEQUEST search engine (Thermo Electron, San Jose, CA, USA). We used the NCBI database (rat, updated at February 2003) and following search parameters: a static modification of carboxyamidomethylation (57 Da) at Cys, a possible modification of GlcNAc (203 Da) at Asn, and trypsin used for digestion.

3. Results

3.1. Extraction of whole proteins from the gel

Rat brain PIPLC-treated GPI-anchored proteins were separated by SDS-PAGE (Fig. 1), and the most noticeable band at 20–25 kDa was cut off from the gel and crushed. The gel pieces were shaken vigorously in 1% SDS, and the extracted protein was precipitated with cold acetone to remove SDS.

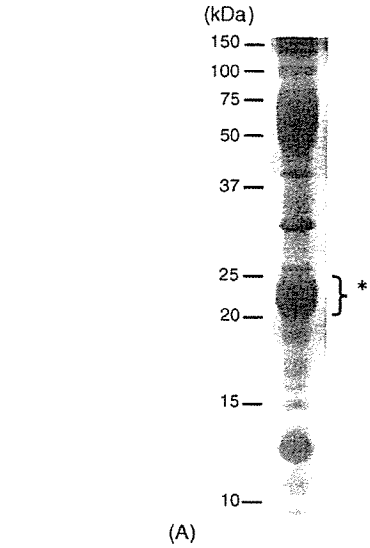

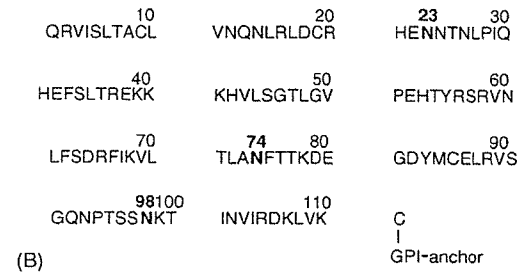

Fig. 1. (A) SDS-PAGE of PIPLC-treated GPI-anchored proteins from rat brain. (B) Amino acid sequence of rat Thy-1. *N*-Glycosylation sites are indicated by bold face. The protein at 20–25 kDa indicated by asterisk was subjected to the glycosylation analysis in this study.

We checked the recovery of the protein at 20–25 kDa by comparing the fluorescence intensity (Ex 633 nm/Em 670 nm) of the proteins at 20–25 kDa visualized by Coomassie staining before and after extraction. Approximately 55% of the protein at 20–25 kDa could be recovered from the gel (data not shown). The protein was digested with trypsin and subjected to the sequential scan consisting of full mass scans with and without in-source CID and data-dependent MS^n by LC/ITMS for protein identification and glycosylation analysis.

3.2. Database search analysis

Fig. 2(A) shows the peptide/glycopeptide map of the trypsin-digested protein at 20–25 kDa. First, all product ions generated by data-dependent MS^n were used for the database search analysis. Using search parameters described in Section 2.5, the protein was identified as Thy-1, a glycoprotein containing three *N*-glycosylation sites at Asn23, 74, and 98, and a GPI attachment site at Cys111. The search analysis also suggested the glycosylation at Asn74 and 98, with elution positions of 34 min (peak T6, Val69-Lys78) and 3.5 min (peak T1, Val89-Lys99), respectively (Fig. 2(A)). Although

Table 1
Glycosylation analysis of rat brain Thy-1

Glycosylation site	Carbohydrate composition[a]				Theoretical carbohydrate mass[b]	Trypsin					Asp-N				
	dHex	Hex	HexNAc	NeuAc		Observed *m/z*	Charge state	Peak number	Amino acid residue[c]	Theoretical *m/z*[b]	Observed *m/z*	Charge state	Peak number	Amino acid residue[c]	Theoretical *m/z*[b]
Asn23	0	5	2	0	1234.43	845.33	3	T3	H21-H31 (1315.63)	845.03	799.47	3	A3	E22-H31 (1178.57)	799.34
						937.27	3	T4	H21-F33 (1591.74)	937.06	1198.69	2	A3	E22-H31 (1178.57)	1198.50
						1405.81	2	T4	H21-F33 (1591.74)	1405.09	949.60	3	A3	N23-T36 (1626.80)	948.75
											1423.40	2	A3	N23-T36 (1626.80)	1422.62
	0	6	2	0	1396.49	899.49	3	T3	H21-H31 (1315.63)	899.04	853.54	3	A3	E22-H31 (1178.57)	853.36
						1348.35	2	T3	H21-H31 (1315.63)	1348.06	1279.66	2	A3	E22-H31 (1178.57)	1279.53
						942.16	3	T3	H21-E32 (1444.67)	942.06	1211.52	2	A5	E22-Q30 (1041.51)	1211.00
						991.37	3	T5	H21-F33 (1591.74)	991.08					
						1486.40	2	T5	H21-F33 (1591.74)	1486.12					
	0	3	5	0	1519.57						1044.43	3	A3	N23-T36 (1626.80)	1043.79
	0	7	2	0	1558.54	996.41	3	T3	H21-E32 (1444.67)	996.07	907.59	3	A3	E22-H31 (1626.80)	907.37
											1361.03	2	A3	E22-H31 (1178.57)	1360.56
	1	3	5	0	1665.62						1093.32	3	A3	N23-T36 (1626.80)	1092.48
	1	5	4	0	1786.65						1133.80	3	A3	N23-T36 (1626.80)	1132.82
	0	6	3	1	1890.66						1168.51	3	A4	N23-T36 (1626.80)	1167.49
	1	6	4	0	1948.70						1187.21	3	A3	N23-T36 (1626.80)	1186.84
Asn74	1	2	3	0	1405.52	1026.26	3	T6	V59-F75 (1996.12)	1026.18					
	0	5	2	0	1234.43	949.52	2	T2	A73-K78 (680.35)	949.39	995.71	3	A7	D64-K78 (1766.01)	995.15
						1162.72	2	T6	V69-K78 (1106.62)	1162.53					
	1	4	3	0	1421.52	1043.45	2	T2	A73-K78 (680.35)	1042.94					
	1	3	4	0	1462.54	1063.68	2	T2	A73-K78 (680.35)	1063.45					
						1276.61	2	T6	V69-K78 (1106.62)	1276.58					
	1	5	3	0	1583.57	1124.18	2	T2	A73-K78 (680.35)	1123.96					
						1337.64	2	T6	V69-K78 (1106.62)	1337.10					
	1	3	5	0	1665.62	1165.13	2	T2	A73-K78 (680.35)	1164.99	1272.15	2	A4	T71-K78 (894.48)	1272.05
						919.71	3	T6	V69-K78 (1106.62)	919.09	1139.79	3	A7	D64-K78 (1766.01)	1138.88
						1378.19	2	T6	V69-K78 (1106.62)	1378.12					
	2	5	3	0	1729.63	1197.53	2	T2	A73-K78 (680.35)	1196.99					
	2	4	4	0	1770.66	1217.67	2	T2	A73-K78 (680.35)	1217.51					
						1430.71	2	T6	V69-K78 (1106.62)	1430.64					
	1	5	4	0	1786.65	1226.38	2	T2	A73-K78 (680.35)	1225.50					
						960.01	3	T6	V69-K78 (1106.62)	959.43					
						1439.05	2	T6	V69-K78 (1106.62)	1438.64					
	1	4	5	0	1827.68	973.79	3	T6	V69-K78 (1106.62)	973.10					
	2	5	4	0	1932.71	1298.75	2	T2	A73-K78 (680.35)	1298.53	1228.18	3	A7	D64-K78 (1766.01)	1227.91
						1008.71	3	T6	V69-K78 (1106.62)	1008.11					
						1512.21	2	T6	V69-K78 (1106.62)	1511.67					
	1	6	4	0	1948.70	1306.81	2	T2	A73-K78 (680.35)	1306.53					
						1013.98	3	T6	V69-K78 (1106.62)	1013.45					
	0	4	5	1	1972.71						1241.91	3	A7	D64-K78 (1766.01)	1241.25
	2	4	5	0	1973.73	880.04	3	T2	A73-K78 (680.35)	879.70	1241.84	3	A7	D64-K78 (1766.01)	1241.59
						1319.24	2	T2	A73-K78 (680.35)	1319.04					
						1022.43	3	T6	V69-K78 (1106.62)	1021.79					
						1532.49	2	T6	V69-K78 (1106.62)	1532.49					

	1	6	3	1	2036.72	1043.24	3	T7	V69-K78 (1106.62)	1042.78					
	1	5	4	1	2077.75	1057.08	3	T7	V69-K78 (1106.62)	1056.46					
	2	6	4	0	2094.76	1062.65	3	T6	V69-K78 (1106.62)	1062.13	1282.43	3	A7	D64-K78 (1766.01)	1281.93
	1	4	5	1	2118.77	1070.38	3	T7	V69-K78 (1106.62)	1070.14					
	2	5	5	0	2135.79	1076.32	3	T6	V69-K78 (1106.62)	1075.81					
	1	6	4	1	2239.80	1110.97	3	T7	V69-K78 (1106.62)	1110.48					
	3	5	5	0	2281.85	1124.78	3	T6	V69-K78 (1106.62)	1124.49					
	1	7	5	0	2313.84	851.76	4	T6	V69-K78 (1106.62)	851.62					
	1	4	6	1	2321.85	1138.16	3	T7	V69-K78 (1106.62)	1137.83					
	2	5	6	1	2629.96	1241.13	3	T7	V69-K78 (1106.62)	1240.53					
Asn98	0	5	2	0	1234.43	1168.34	2	T1	V89-K99 (1117.54)	1167.99	912.24	3	A2	E86-K99 (1515.76)	911.74
											1367.31	2	A2	E86-K99 (1515.76)	1367.10
											930.26	3	A3	Q92-R105 (1570.84)	930.10
											1021.28	3	A3	E86-N102 (1843.94)	1021.13
											1011.53	3	A4	T95-K110 (1815.06)	1010.81
											1516.43	2	A4	T95-K110 (1815.06)	1516.75
											1144.21	3	A5	E86-R105 (2212.18)	1143.88
	0	3	4	0	1316.49	1209.79	2	T1	V89-K99 (1117.54)	1209.02					
	0	3	5	0	1519.57	1310.68	2	T1	V89-K99 (1117.54)	1310.56	1007.10	3	A2	E86-K99 (1515.76)	1006.78
											1106.39	3	A4	T95-K110 (1815.06)	1106.55
											1239.21	3	A5	E86-R105 (2212.18)	1238.92
	2	3	4	0	1608.60						951.28	3	A4	G91-N102 (1259.61)	951.08
											1426.22	2	A4	G91-N102 (1259.61)	1426.11
	1	4	4	0	1624.60	951.37	3	T3	S96-D106 (1245.67)	951.76					
	0	5	4	0	1640.59	1371.84	2	T1	V89-K99 (1117.54)	1371.07	960.04	4	A5	E86-R105 (2212.18)	959.70
											1279.69	3	A5	E86-R105 (2212.18)	1279.26
	0	5	3	1	1728.61						1176.27	3	A4	T95-K110 (1815.06)	1176.23
	0	5	4	0	1640.59						1146.70	3	A4	T95-K110 (1815.06)	1146.89
	1	6	3	0	1745.62						1082.52	3	A2	E86-K99 (1515.76)	1082.13
											1181.80	3	A4	T95-K110 (1815.06)	1181.90
											986.38	4	A5	E86-R105 (2212.18)	985.96
											1314.72	3	A5	E86-R105 (2212.18)	1314.27
	1	5	4	0	1786.65						1195.47	3	A4	T95-K110 (1815.06)	1195.57
											996.54	4	A5	E86-R105 (2212.18)	996.21
											1328.49	3	A5	E86-R105 (2212.18)	1327.95
	1	5	3	1	1874.67						1018.89	4	A6	E86-R105 (2212.18)	1018.22
	0	6	3	1	1890.66	1496.18	2	T1	V89-K99 (1117.54)	1496.10	1230.24	3	A4	T95-K110 (1815.06)	1230.24
											1022.70	4	A6	E86-R105 (2212.18)	1022.22
	2	5	4	0	1932.71	1517.35	2	T1	V89-K99 (1117.54)	1517.13					
	1	6	4	0	1948.70	1525.78	2	T1	V89-K99 (1117.54)	1525.12	1150.13	3	A2	E86-K99 (1515.76)	1149.83
											1249.75	3	A4	T95-K110 (1815.06)	1249.59
											1259.45	3	A3	E86-N102 (1843.94)	1259.22
											1037.27	4	A5	E86-R105 (2212.18)	1036.73
											1382.34	3	A5	E86-R105 (2212.18)	1381.97
	1	6	3	1	2036.72						1059.07	4	A6	E86-R105 (2212.18)	1058.73
	0	6	4	1	2093.74						1298.06	3	A4	T95-K110 (1815.06)	1297.94
											1073.37	4	A6	E86-R105 (2212.18)	1072.99

[a] dHex, deoxyhexose; Hex, hexose; HexNAc, *N*-acetylhexosamine; NeuAc, *N*-acetylneuramic acid.
[b] Monoisotopic value.
[c] Theoretical peptide mass is indicated in parenthesis.

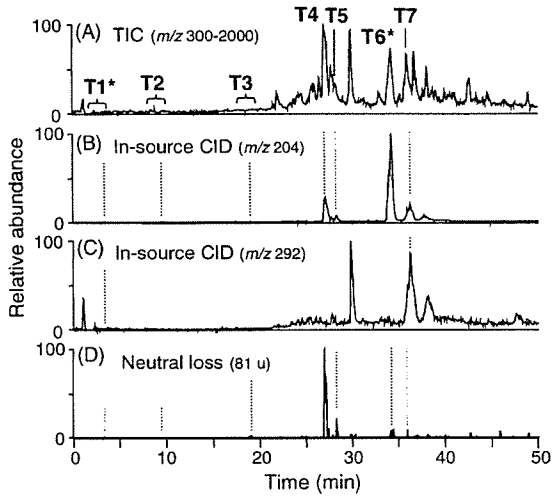

Fig. 2. Total ion chromatogram (TIC) of trypsin-digested protein at 20–25 kDa (*m/z* 300–2000) (A), mass chromatograms from TIC with in-source CID of *m/z* 204 (B) and 292 (C), and neutral loss chromatogram of 81 u by data-dependent CID-MS/MS (D). Asterisks mean the peak of glycopeptides identified by the database search analysis.

the glycopeptide Val89-Lys99 contains two Asn residues, Asn93 and 98, only Asn98 was identified as a glycosylation site because of detection of b and y ions modified with GlcNAc at Asm98.

Next, to study the site-specific glycosylation at Asn74 and 98, product ion spectra of glycopeptides were sorted from the numbers of product ion spectra acquired around peak T6 and T1. We sorted out product ion spectra of glycopeptides using B series ions, such as $Hex_1HexNAc_1^+$ and $Hex_2HexNAc_1^+$ (*m/z* 366 and 528) originated from glycopeptides by CID-MS/MS, as marker ions [23]. We could sort out 14 product ion spectra originated from glycopeptide Val69-Lys78 around peak T6. The monosaccharide compositions of *N*-glycans at Val69-Lys78 were calculated as $dHex_{0-3}Hex_{2-7}HexNAc_{2-5}$ on the basis of the *m/z* values of their molecular ions and the theoretical mass of the peptide. Likewise, seven product ion spectra originated from glycopeptide Val89-Lys99 were sorted from those around peak T1, and their monosaccharide compositions were estimated as $dHex_{0-2}Hex_{3,5,6}HexNAc_{2-5}NeuAc_{0,1}$ (Table 1). Glycosylation at Asn74 and 98 were elucidated by a detailed examination of these product ion spectra as follows.

3.2.1. Analysis of the glycosylation at Asn74 of peptide Val69-Lys78

Fig. 3(A) shows a product ion spectrum of the glycopeptide Val69-Lys78 at 34.52 min. Its precursor ion is the doubly charged ion at *m/z* 1512.2. Many product ions generated by cleavages of glycosidic linkages can be observed in this product ion spectrum. The most intense ion at *m/z* 1311 is assigned to a peptide bearing the reducing end of GlcNAc, which was caused by glycosidic linkage cleavage of *N*-linked oligosaccharide. Fig. 3(B) is the product ion spectrum of the peptide + GlcNAc ion at *m/z* 1311. The b and y ions generated by cleavages of the peptide backbone prove that this glycopeptide is the peptide Val69-Lys78 glycosylated at Asn74.

The molecular weight of the carbohydrate moiety can be calculated as 1933.8 Da by subtracting the theoretical mass of the peptide (1106.6 Da) from the calculated glycopeptide mass (3022.4 Da). Consequently, the monosaccharide composition can be estimated as $dHex_2Hex_5HexNAc_4$. In the product ion spectrum (Fig. 3(A)), B ions corresponding to $dHex_1Hex_1HexNAc_1$ ($B_{2\alpha}$) and $dHex_1Hex_2HexNAc_1$ ($B_{3\alpha}$) were detected at *m/z* 512 and 674, respectively. These results indicate that one of two dHex, which are likely to be Fuc, attaches to Gal-GlcNAc at the non-reducing end in a similar manner as the Lewis a/x antigen (Gal-(Fuc-)GlcNAc-), or the blood group H-determinant (Fuc-Gal-GlcNAc-). The product ion at *m/z* 350 produced from the triply charged precursor ion at *m/z* 1008.7 corresponded to $dHex_1HexNAc_1$ (data not shown), suggesting that Fuc attaches to GlcNAc like the Lewis a/x antigen (Gal-(Fuc-)GlcNAc-). The attachment site of the other Fuc can be deduced at inner trimannosyl core GlcNAc from the observation of Y ions at *m/z* 1457, 1660, and 1822, which correspond to Val69-Lys78 plus $dHex_1HexNAc_1$ ($Y_{1\alpha}$), $dHex_1HexNAc_2$ ($Y_{2\alpha}$), and $dHex_1Hex_1HexNAc_2$ ($Y_{3\alpha/3\beta/3\gamma}$), respectively. In addition, the product ion at *m/z* 1411 resulting from the precursor ion at *m/z* 1512.2 by loss of 101.6 u (HexNAc), suggests a linkage of non-substituted HexNAc at the non-reducing terminal end. Together with detection of the product ion at *m/z* 940 ($Y_{3\alpha/1\beta/3\beta}^+$, [GlcNAc-Man-GlcNAc-GlcNAc-peptide+H]$^{2+}$), it can be deduced that this HexNAc is a bisecting GlcNAc attached to the core mannose residue via a β1–4 linkage. From these product ions, we could deduce two oligosaccharide structures. One is the structure indicated in Fig. 3(A), inset, and the other is one containing a Gal-Gal-(Fuc-)GlcNAc-Man-branch instead of a Gal-(Fuc-)GlcNAc-Man-branch. Detection of Gal-(Fuc-)GlcNAc-Man$^+$ at *m/z* 674 but not Gal-Gal-(Fuc-)GlcNAc-Man$^+$ at *m/z* 836 suggests that this oligosaccharide structure can be assigned to the structure indicated in Fig. 3(A), inset.

The carbohydrate structures of the other glycopeptide Val69-Lys78 detected around peak T6 can be characterized as the high-mannose-type oligosaccharide (M5), complex-type oligosaccharides containing some partial structures such as inner core Fuc, bisecting GlcNAc, the Lewis a/x antigen, and blood group H-determinant, and hybrid-type oligosaccharides (Table 1).

3.2.2. Analysis of the glycosylation at Asn98 of peptide Val89-Lys99

Fig. 4 shows one of the product ion spectra of the glycopeptide Val89-Lys99 at 3.47 min. Its precursor ion is the doubly charged ion at *m/z* 1525.8. The monosaccharide composition, $dHex_1Hex_6HexNAc_4$, can be estimated based on the calculated mass of the carbohydrate moiety (1950.0 Da) obtained by subtracting the mass of the theo-

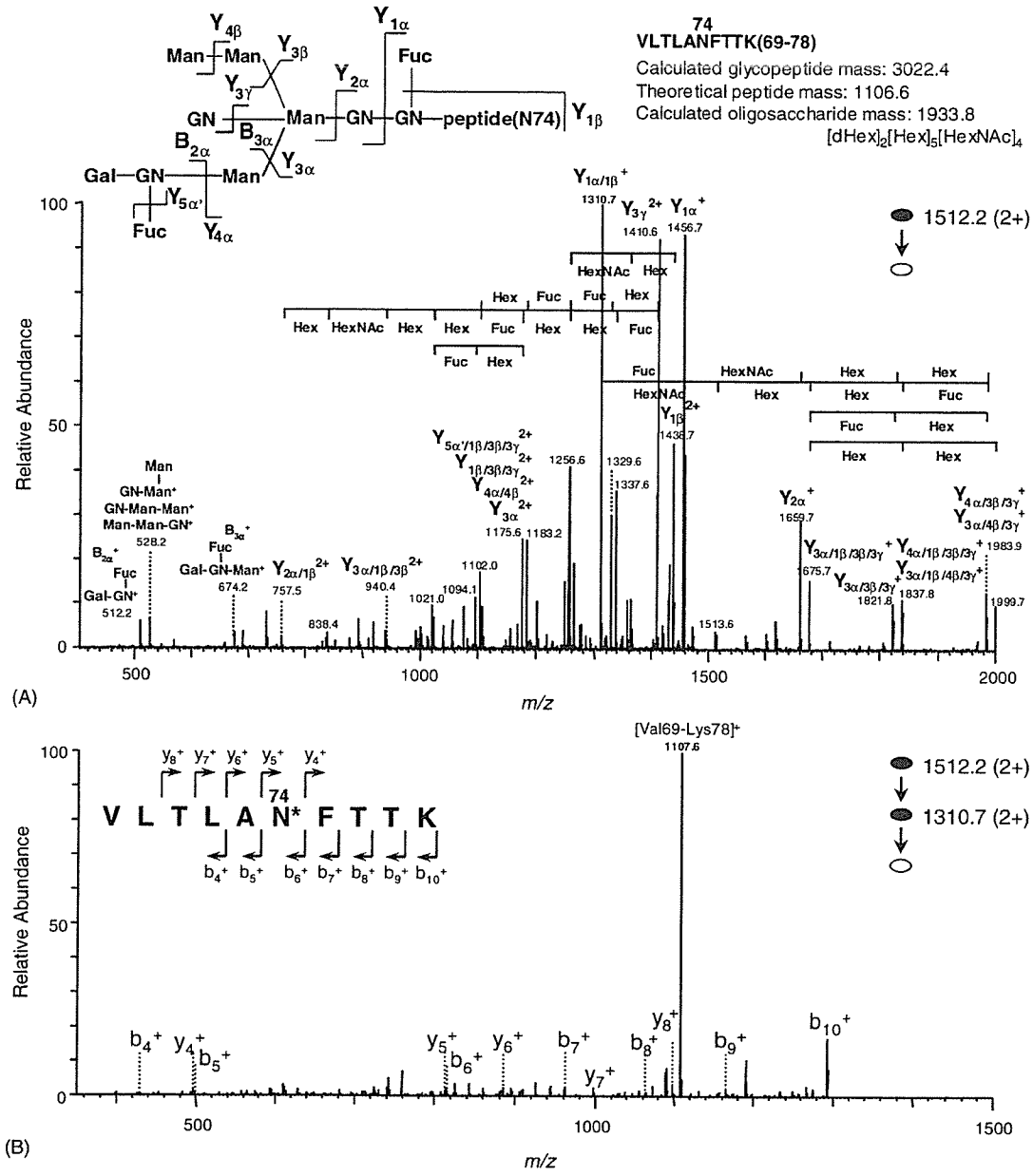

Fig. 3. (A) Product ion spectrum (MS^2) of the doubly charged glycopeptide precursor ion at *m/z* 1512.2 in peak T6. The glycopeptide Val69-Lys78 is glycosylated with oligosaccharide, $dHex_2Hex_5HexNAc_4$ at Asn74, and the inset is the deduced oligosaccharide structure. (B) MS^3 product ion spectrum derived from the doubly charged glycopeptide precursor ion at *m/z* 1512.2, followed by further fragmentation of the product ion at *m/z* 1310.7.

retical typtic peptide mass (1117.5 Da) from the calculated glycopeptide mass (3049.5 Da). Y ions corresponding to Val89-Lys99 plus $dHex_1HexNAc_1$ ($Y_{1\alpha}$), $dHex_1HexNAc_2$ ($Y_{2\alpha}$), and $dHex_1Hex_1HexNAc_2$ ($Y_{3\alpha/3\beta/3\gamma}$) detected at *m/z* 1468, 1671, and 1833, respectively, reveals that one Fuc residue is linked to the inner trimannosyl core GlcNAc. Additionally, the product ion at *m/z* 1424 suggests a linkage of non-substituted HexNAc at the non-reducing terminal end. Together with the product ions at *m/z* 945 and 1890, it can be deduced that this HexNAc is a bisecting GlcNAc that attaches to a core mannose residue via a β1–4 linkage. On the basis of the product ions at *m/z* 487, 528 and 1380, corresponding to Hex_3 ($B_{2\beta}$), $Hex_2HexNAc_1$ ($B_{3\alpha}$), and $Hex_6HexNAc_2$ ($B_{4\alpha}$), the oligosaccharide structure was characterized as a hybrid-type oligosaccharide (Fig. 4, inset).

The carbohydrate structures of the other glycopeptide Val89-Lys98 detected around peak T1 are characterized as high-mannose-type oligosaccharide (M5), complex-type, and hybrid-type oligosaccharides, which include bisecting GlcNAc and Lewis a/x structures (Table 1).

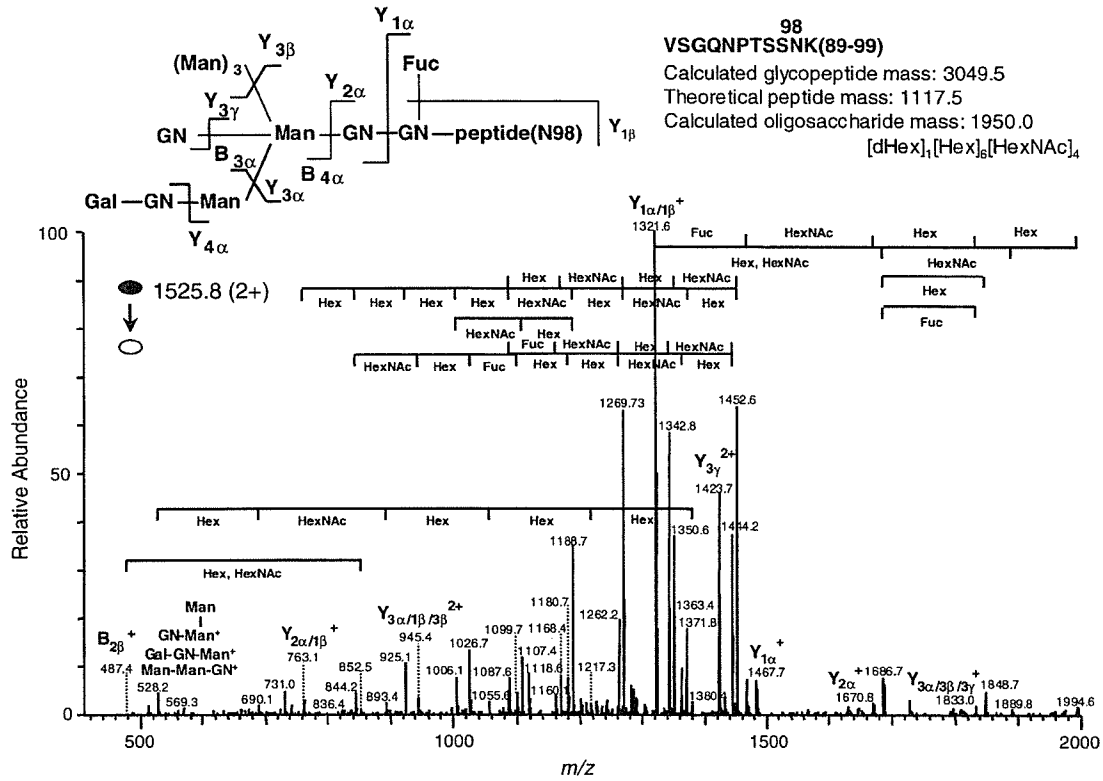

Fig. 4. Product ion spectrum of the doubly charged glycopeptide precursor ion at *m/z* 1525.8 in peak T1. The glycopeptide Val89-Lys99 is glycosylated with the oligosaccharide, $dHex_1Hex_6HexNAc_4$ at Asn98, and the inset is the deduced oligosaccharide structure.

3.3. Detection of glycopeptides by in-source CID and CID-MS/MS

Glycopeptides containing Asn23 could not be identified by the database search analysis. Therefore, we first localized all glycopeptides in the peptide/glycopeptide map using oxonium marker ions generated by in-source CID. Fig. 2(B and C) shows mass chromatograms of oxonium marker ions, $HexNAc^+$ (*m/z* 204) and $NeuAc^+$ (*m/z* 292), respectively. The mass chromatogram of *m/z* 204 indicates that the glycopeptides were localized around 3.7, 9.7, 19.1, 27.2, 28.4 34.3, 36.3, and 37.8 min. The mass chromatogram of *m/z* 292 suggests that the glycopeptides bearing NeuAc were localized around 3.7, 30.0, 36.4, and 38.2 min. In addition to the localization of glycopeptides by in-source CID, we monitored neutral loss caused by data-dependent CID-MS/MS. The neutral loss chromatogram of 81 u indicates the localization of doubly charged glycopeptides ions with Hex at the non-reducing ends. The elution positions of the localized glycopeptides by neutral loss are almost identical to those by in-source CID. Second, for confirmation of the elution position of glycopeptides and characterization of the carbohydrate moiety, we sorted the product ion spectra of glycopeptides from enormous numbers of data-dependently acquired product ion spectra around localized glycopeptides by using oligosaccharide oxonium ions as marker ions. Consequently, the locations of glycopeptides were confirmed in peak T1-6 (Fig. 2(A)). The peaks T1 and 6 correspond to the location of glycopeptides identified by the database search as Val89-Lys99 and Val69-Lys78, respectively. Four glycopeptide peaks were newly sorted by in-source CID and data-dependent CID-MS/MS. Structural assignment of the glycopeptides in these peaks was carried out using their MS^n spectra as follows.

3.3.1. Analysis of the glycosylation at Asn23 of peptide His21-Phe33

Fig. 5(A) shows one of the product ion spectra of the glycopeptide His21-Phe33 in peak T4. Its precursor ion is the triply charged ion at *m/z* 937.3. The intense product ion at *m/z* 899 is assigned to a doubly charged ion of peptide plus GlcNAc on the basis of Y series ions. The region of His21-Phe33 containing Asn23 in Thy-1 was suggested as the peptide moiety of this glycopeptide, 1593.3 Da, by the FindPept tool available on the internet (ExPASY Proteomics tools, Swiss Institute of Bioinformatics, http://us.expasy.org/tools/findpept.html). We examined the data-dependently acquired product ion spectrum of the precursor ion at *m/z* 899 and found that the *m/z* values of b and y ions in the product ion spectrum were identical to those of predictable product ions originating from the peptide His21-Phe33 modified with HexNAc at Asn23 (Fig. 5(B)). From the calculated oligosaccharide mass (1235.1 Da) obtained by subtracting the theoretical typtic

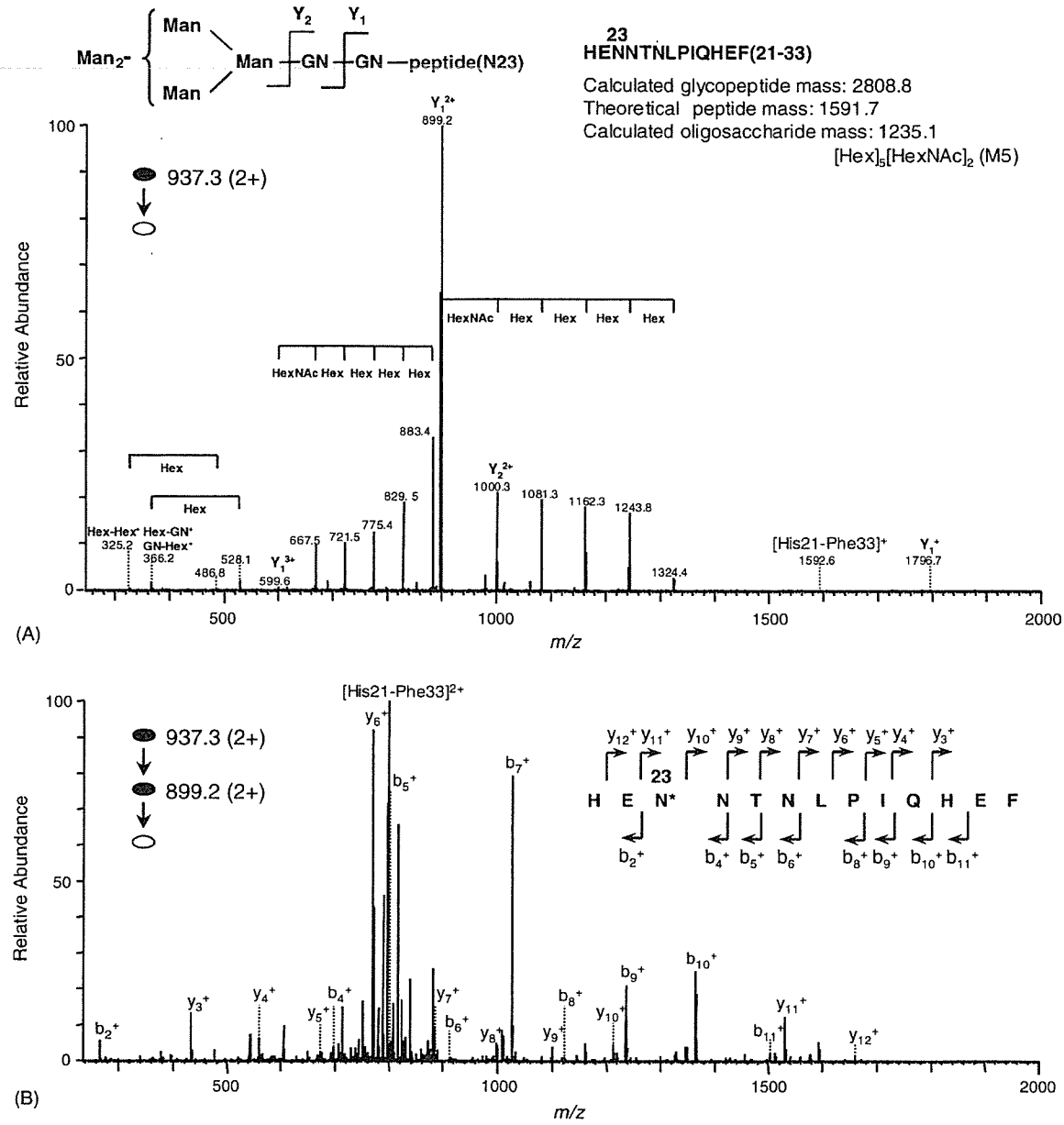

Fig. 5. (A) Product ion spectrum (MS^2) of the doubly charged glycopeptide precursor ion at *m/z* 937.3 in peak T4. The glycopeptide His21-Phe33 is glycosylated with oligosaccharide, $Hex_5HexNAc_2$ at Asn23, and the inset is the deduced oligosaccharide structure. (B) MS^3 product ion spectrum derived from a doubly charged glycopeptide precursor ion at *m/z* 937.3, followed by further fragmentation of the product ion at *m/z* 899.2.

peptide mass (1591.7 Da) from the calculated glycopeptide mass (2808.8 Da) together with product ions at *m/z* 366 and 528, it is indicated that this peptide carries $Hex_5HexNAc_2$, i.e. high-mannose-type oligosaccharide, M5. All product ion spectra in peak T4 revealed that peptides His21-Phe33 contain only high-mannose-type oligosaccharide (M5).

3.3.2. *Analysis of glycopeptides in peaks T2, 3, 5, and 7*

Similarly, product ion spectra of glycopeptides around peaks T2, 3, 5, and 7 were sorted by using oligosaccharide oxonium marker ions generated by MS/MS. In product ion spectra sorted out from around peak T2, the intense ion at *m/z* 884 was detected and assigned to a singly charged ion of a peptide plus GlcNAc. The peptide was suggested to be Ala73-Lys78 containing Asn74 by the FindPept tool. The monosaccharide composition can be estimated from the calculated mass of oligosaccharide moiety obtained by subtracting the theoretical mass of Ala73-Lys78 (680.35 Da) from calculated glycopeptide mass. Oligosaccharide structure of the glycopeptides is characterized based on their product